UiT
THE ARCTIC
UNIVERSITY
OF NORWAY

Department of Physics and Technology

Optimization of a polymer layer highly doped with Cryptophane-A for methane sensing

—
Mukesh Yadav

FYS-3900 Master's thesis in Physics- May 2017

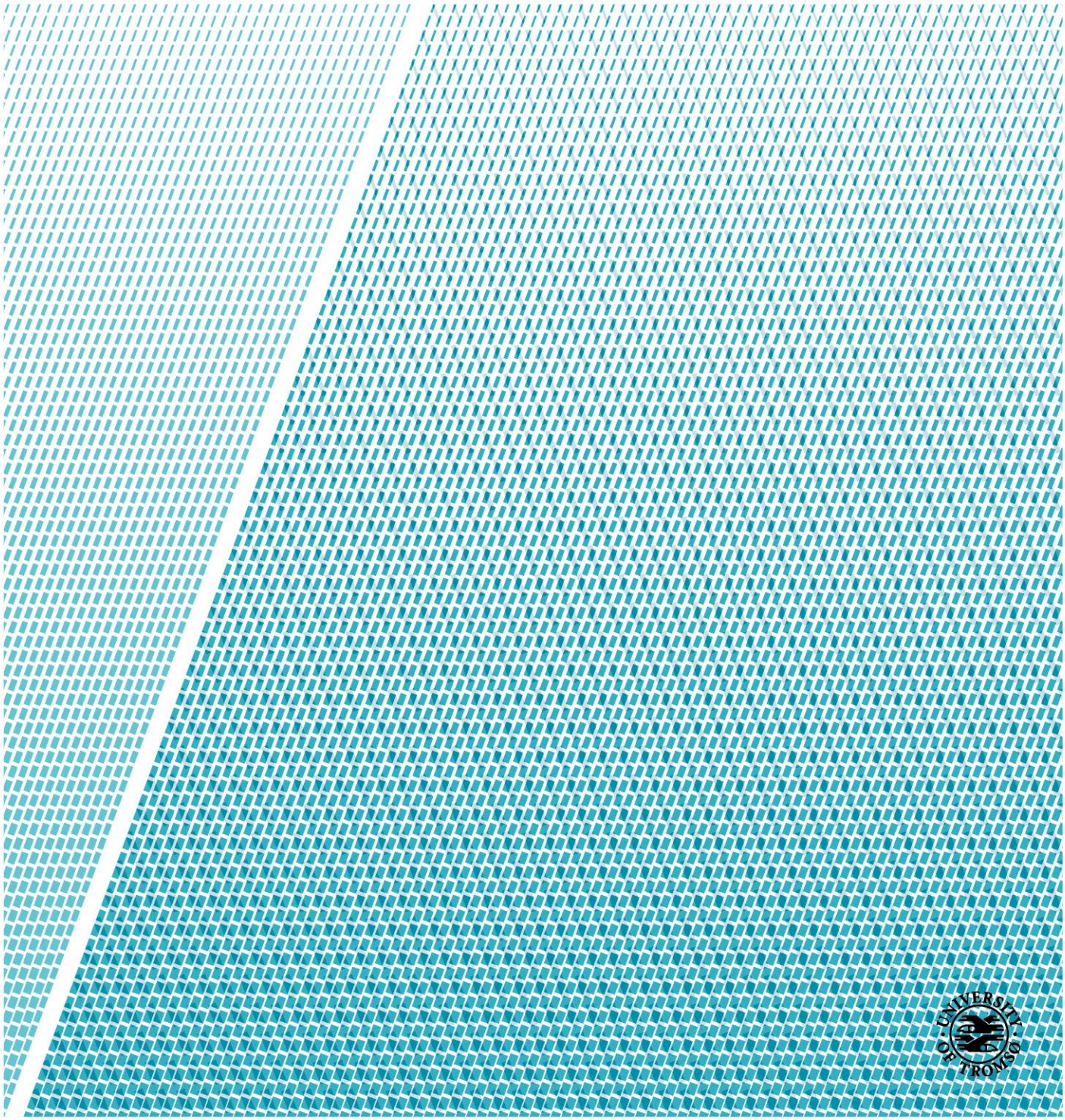

Abstract

The main objective of this thesis is to optimize the thickness of sensitive polymer layer highly doped with Cryptophane-A for methane pre-concentration and to make the existing sensor more stable and selective towards methane.

In recent years, methane detection has become a hot topic due to the strong impact of methane on the global warming and the climate change. There has also been rising interest in the development of new methane sensors that can tackle the task of sensitive atmospheric methane detection, but are smaller, lighter, and cheaper than the state of the art. Our approach to this challenge is the development an on-chip waveguide sensor, which compensates for the rather short path lengths possible on a chip with pre-concentration of methane in a thin, specially designed waveguide cladding layer.

Our detection technique is based on evanescent refractive index sensing with a Silicon Nitride shallow rib-waveguide Mach-Zehnder interferometer. The waveguide was fabricated with dimensions supporting single TE and TM modes at the wavelength of 785 nm. The reference arm is cladded with SiO_2 that is impermeable to methane, and the sensing arm is cladded with Styrene Acrylonitrile (SAN) polymer doped with Cryptophane-A. Cryptophane-A is a molecular compound, which has a high affinity towards methane. The sensor group have previously reported that the presence of cryptophane increases the methane concentration in the SAN layer. The limit of detection of existing set-up is 6 ppm.

However, to bring the methane sensor to the field, not only sensitivity but also specificity to methane and the sensor response time need to be quantified. In this thesis, both parameters were targeted.

First, the sensor was characterized for sensitivity and response time of different thicknesses of sensitive layer with Cryptophane-A: SAN concentration of 8.5. The measurement result shows that both sensitivity and response time increase with thickness. The sensitivity gets saturated at 400 nm while response time continues to increase.

Second, the measurement was done to reach the limit of sensitivity of developed sensor. The measurement result shows that the sensitive layer of Cryptophane-A: SAN concentration of 1:1 gives the highest sensitivity. Then measurement was done for thin layer of highest sensitive

layer and PDMS on top of that. The measurement result shows that sensitivity is increased to twice of previous reported value and response time reduced by almost 3 times.

At the end, the drift in the sensor was reduced by deposition of SAN on one arm and SAN doped with cryptophane-A on the other. The measurement data shows that the long-term drift which was evident when SiO_2 was cladded in one arm is reduced. The deposition of polymer on both arms also provides specificity towards methane.

The specificity, high sensitivity, fast response and stability makes it a robust sensor that can be mounted on drone (UAV) for real-time testing.

Acknowledgement

First of all, I would like to thank my supervisor, Dr. Jana Jágerská, and my co-supervisor, Professor Olav Gaute Hellesø, for their continuous support, guidance, healthy discussions and encouragement during my master's thesis.

I would like to thank Dr. Jana Jágerská for her simulations of effective refractive index and sensitivity.

I am heartily thankful to you Dr. Firehun Tsige Dullo for strong discussions and frank exchange of ideas during my thesis.

I am also grateful to Dr. Habib for his support and clean room training.

I am sincerely thankful to our optics group members for their healthy discussion on project during meetings as well as personally.

I would like to thank Department of physics, University of Tromsø, Norway for providing me an opportunity to work on a very interesting project and I would also like to thank Department of chemistry, UiT for fabrication of cryptophane-A.

Finally, I would like to thank my family members and friends for their continuous support and encouragement.

Table of Contents

Chapter 1

Introduction

1.1 Motivation

In recent years, the global warming has become a hot topic as earth temperature has increased by 0.8°C over past hundred years and it is expected to increase by 0.3°C to 4.8°C over the next century [1]. The rise in global temperature is now causing the climate changes resulting in drought in some places and floods in others. Glaciers and oceans are also getting affected by the global rise in temperature, the sea level is rising and the oceans are becoming more acidic.

Greenhouse gasses are responsible for the rise in global warming as these gases like CO_2, CH_4, CFC, N_2O, etc. tend to trap the radiation coming from the sun, which warms the earth atmosphere. Each of these gases has a specific global warming potential, which defines the capacity of a gas to cause global warming. Global warming potential (GWP) is defined as the energy absorption by 1 ton of gas over a given time relative to energy absorption by the 1 ton of CO_2. Carbon dioxide is taken as the reference gas and has by definition global warming potential of 1. It stays in the atmosphere for thousands of years. Methane gas has approx. 28-30 GWP over 100 years which is very high in comparison to carbon dioxide. Some gases like N_2O, CFCs have GWP in the range from 100 to 2000 on the 100-year scale relative to CO_2, but the concentration of these gases in the atmosphere is very low [1].

Methane gas has high global warming potential and its concentration in the atmosphere in comparison to other greenhouse gases (except carbon dioxide) is also high. It has a short lifetime in comparison to Carbon dioxide which results in 28-30 GWP on a 100-year scale but on a 20-year scale, it is around 84-87. The main sources of methane emission are the agriculture sector (animals like cows, buffalos, sheep, goats, and camels produce a lot of methane), natural gas processing, landfills, and wetlands. The methane gas concentration in the atmosphere was slowly increasing from 1983-1999 and was constant from 1999-2006. After 2007 it is again increasing. In recent years, 2014-2015, the concentration of methane increased at a very fast rate (11 ppb/year) [2].

In recent years, rise in the arctic temperature and increased rainfall in tropical wetlands resulting in increase in concentration of methane in atmosphere. Because rise in the arctic temperature leads the melting of the arctic ice where large quantity of methane is present in the form of frozen permafrost. Similarly, the rainfall in tropical wetlands results in the emission of methane from the soil due to ebullition process which is defined as the release of methane bubbles from soil [2].

Wetlands and the arctic lakes are one of the largest emitter of methane [3]. But the contribution of these emitters is not precisely known because of their location and lack of reliable measurement devices. At present, a lot of small and cheap methane sensor are available that are used for detection of methane in remote areas using drones, but they are less sensitive and not stable enough to provide precise information of methane concentration. Some highly stable and highly sensitive methane sensors are also available but they are very big and used only in laboratory. So, we need a high sensitive, compact and robust methane sensor that can be used to do continuous monitoring of methane in remote areas.

At present, various kinds of gas sensing technologies are in use for detection. Broadly speaking, detection technologies are divided into detection based on change in electrical properties and changes in other properties (optical, chromatography etc.) [4]. Metal Oxide Semiconductors, Polymer, Carbon Nanotubes sensors are based on variation in electrical properties for different gases. Optical and chromatographic sensors are based on change in optical and chromatographic properties for different gases. These techniques have their specificities and limitations. Electrical sensors are low cost, fast, and applicable for wide range of gases but they are less sensitive and selective than optical and chromatographic sensors. The limitation with chromatographic sensor is that, they are very expensive and not portable. In the other hand, optical sensors have big advantage over chromatographic sensor that, optical sensors can be miniaturized so, it can be used for continuous monitoring of methane gas in remote areas using drone. Optical gas sensors are divided into different categories based on which optical technique is used e.g. laser spectroscopy, refractive index sensing and surface plasmon resonance etc.

It will be shown that the optical gas sensors based on evanescent field sensing using waveguide has the potential to fulfill all the requirements for a robust, cheap, portable and highly sensitive methane sensor.

1.2 Aim

The aim of the project (Sensor Technology WP1) is to develop a robust, highly sensitive, portable and fast methane sensor using a waveguide Mach-Zehnder interferometer. The plan is to mount this sensor on a drone and use it to measure methane in remote areas.

The aim of this M.Sc. project is to optimize the layer of cryptophane-A doped SAN polymer for high sensitivity and fast response time. And to improve the stability and the selectivity of existing methane sensor.

Chapter 2

Principles

2.1 Optical sensors

The optical sensor technology has become very popular over recent decades. Optical sensors are now commonly used in oil and gas industries, defence industry, healthcare and environmental monitoring. Optical sensors are getting popular over other technologies as they can provide very high sensitivity, high stability, in-situ measurements, safety operations and fast response time that makes it useful for real-time monitoring. But optics also have some disadvantages of being fragile, expensive and the requirement of clean surface.

There are various techniques used in optical sensing with different inherent limitations and applicability. Some of the common techniques are laser spectroscopy, Surface Plasmon resonance [16], interferometry [9], etc. Laser spectroscopy is a general term which includes various techniques for e.g. Raman spectroscopy, Absorption spectroscopy, laser induced fluorescence spectroscopy etc. In laser spectroscopy techniques, the interaction of laser with the desired material is utilized as the sensing parameter which is sometimes measured as the function of frequency or wavelength for e.g. in absorption spectroscopy, after the interaction of laser with desired material the measure of absorption of laser radiation as a function of wavelength or frequency. The surface Plasmon resonance technique is based on total internal reflection (section 2.2), electromagnetic field at metal and dielectric interface used to detect the index change in sample. SPR is commonly used for bio sensing application. The interferometric (Mach-Zehnder and Young's interferometer) sensors are also common in chemical and bio sensing. The interferometric sensors utilize the output phase change as a sensitivity parameter.

2.2 Waveguide sensors

Optical fiber and waveguides are based on the principle of total internal reflection. Total internal reflection (TIR) is defined as the phenomenon in which light get reflected in higher refractive index medium (n_1) surrounded by low refractive index medium (n_2), if the angle of incidence is greater than critical angle (θ_c) as shown in fig. 2.1 (right).

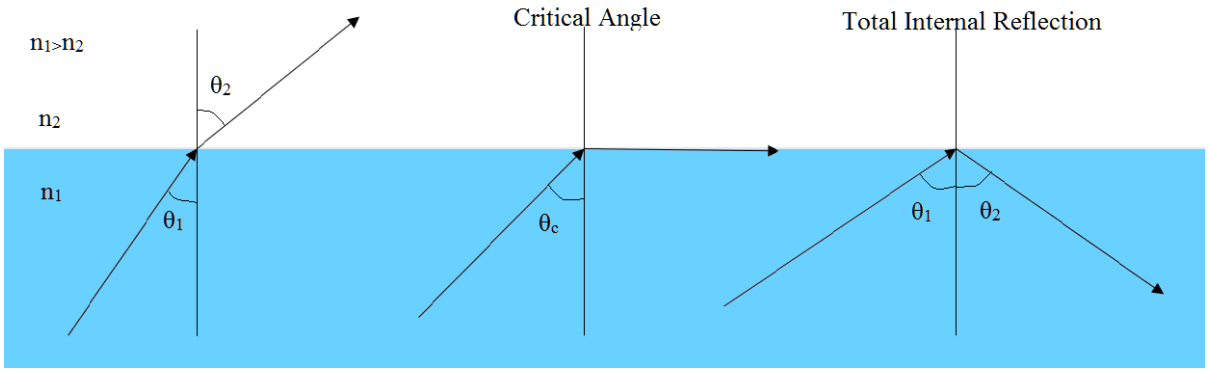

Fig. 2.1 Condition for total internal reflection

The guiding of light in optical fiber and waveguide under total internal reflection is shown in Fig. 2.2. Optical fibers are usually in the cylindrical shape with core of higher refractive index medium (n_1) and cladding with low refractive index medium (n_2). And similarly, waveguides are rectangular in shape with higher refractive index medium (n_1) as a core which is sandwiched between two low refractive index media (n_2, n_3).

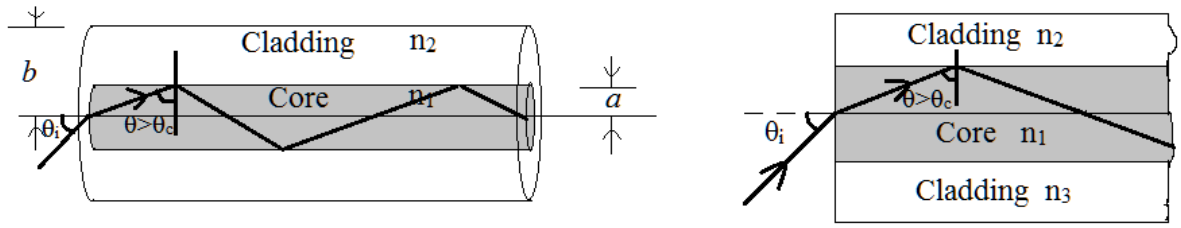

Fig. 2.2 Optical fiber (left) and optical waveguide (right)

In the waveguide and the optical fibers, light undergoes multiple reflections in core medium. In order to get confined light in the waveguide, the reflecting waves must satisfy a self-consistency condition which requires that the wave reproduces itself after twice reflections in the waveguide. And the fields satisfying this self-consisting condition are called the modes of the waveguide. Modes are defined as the fields which maintain the same distribution and polarization along the waveguide. The waveguide and the optical fiber supports single mode and multimode both fields, which depends on the waveguide refractive index and dimensions for particular wavelength.

In initial stage, the waveguide and the optical fiber were used in the optical telecommunication [5, 9]. But, since the development of the semiconductor laser and the single mode fiber. The optical fibers have been in use for sensing of physical variables for e.g. Temperature, pressure, strain etc. [14]. These sensors are based on various optical techniques for e.g. Braggs grating, fluorescence, and spectroscopy. Flexibility of this fiber gives advantage of multi-point sensing over range of several kilometers. Military, power generation, oil and gas, environment and health care industries are leading user of fiber optic sensors [6]. Fiber optic sensor also have some advantages for e.g. High level of noise, less stable and highly sensitive. Then, advancement in integrated optics encouraged development of planar waveguides as sensors. The small size of planar optical waveguides provides an advantage over optical fibers for on-chip and also the better stability. Optical waveguides can be designed in a specific manner to get low bending losses, low propagation losses [7]. Single mode optical waveguides with large refractive index between core and cladding provides higher sensitivity in comparison to fiber and multimode waveguide sensor as it offers high field intensity at surface. While, low contrast waveguides provide long penetration depth of decaying field in cladding, which is commonly used in sensing application, termed as evanescent field sensing (section 2.2.1). Optical waveguides are typically fabricated by thin film deposition. Silicon nitride, tantalum pentoxide and another high index materials are deposited on a substrate with low index [8]. Waveguide sensor are very popular in chemical and bio sensing application and most of the sensors are based on evanescent field sensing, with a sensitive layer (cladding) deposited on a core layer and thus interacting with the evanescent field [8-10, 12, 19-21]. The refractive index of the sensitive layer changes when exposed to specific measurand e.g. Methane. To detect the effective refractive index change in a sensitive layer, Mach-Zehnder interferometer (section 2.2.2), Young interferometer, bimodal interferometer [13] are used. These interferometers detect refractive index change in the form of phase change at the output.

This thesis is focused on evanescent field sensing of methane using Mach-Zehnder interferometer made with optical waveguide [11].

2.2.1 Evanescent field sensing

At the boundary, between dielectric mediums waveguide and cover, tangential component of E and H fields must be continuous. For electromagnetic wave propagating along z direction in asymmetric waveguide, E_Y and H_Z must be continuous at interface between waveguide and cover to get TE polarization. Along with guided light in waveguide, fast decaying electromagnetic field surrounds the waveguide. This fast decaying field in cover region is known as evanescent field. Which is given as;

$$E_y(x,z) = E_{y0}e^{-\alpha x}$$

where E_{y0} is the electric field at interface, x is the distance in cover and α is the attenuation coefficient which is given as:

$$\alpha = k_0 \sqrt{n^2{}_{eff} - n^2{}_1}$$

where n_{eff} is effective index of the mode, n_1 is the refractive index of cover and $k_0 = {}^{2\pi}/_{\lambda}$.

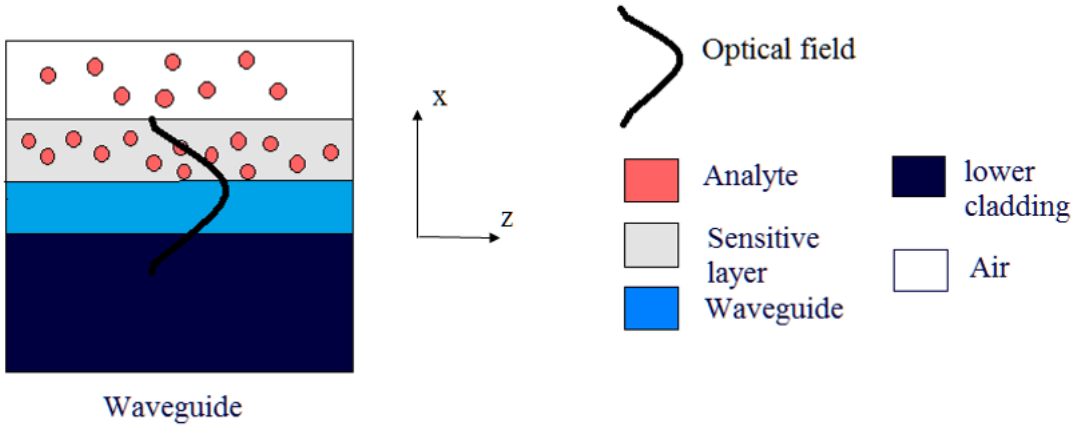

Fig 2.3 Schematic diagram of evanescent field sensing

In the evanescent field sensing, the evanescent field interacts with the absorption and the density change in cover region which results into the change in effective refractive index of the guided mode in the waveguide. Typically, evanescent field extends for few 100 nm in cover region but it can be increased to 1 µm by increasing the refractive index of cover region. The increase in depth of evanescent field in cover region increases the sensitivity as it increases the interaction of analyte with electromagnetic field.

2.2.2 Mach-Zehnder Interferometer

The waveguide Mach-Zehnder interferometer sensor is based on the principle of interference of the modes in two single mode optical waveguide. The Mach-Zehnder interferometer has an input waveguide that is divided into two by using a Y-junction. One arm acts as reference arm and the other as sensing arm. After a specific length, the waveguides are recombined using Y-

junction as shown in Fig.2.4.

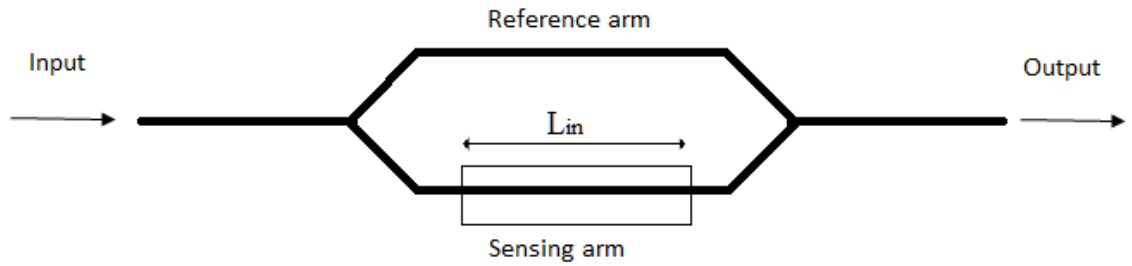

Fig.2.4 Outline of Mach-Zehnder interferometer

The sensing arm is cladded with a sensitive layer and reference arm is cladded with a layer that is insensitive to measurand.

A waveguide Mach-Zehnder interferometer must have single mode waveguide to give high visibility.

The effective refractive index change in the sensing arm due to measurand leads to the phase change at the output. Phase change at the waveguide output can be directly calculated from the waveguide output intensity as:

$$I = I_s + I_r + 2\sqrt{I_s I_r}\cos(\Delta\varphi_m)$$

$$\Delta\varphi_m = cos^{-1}((I - I_r - I_s)/2\sqrt{I_s I_r})$$

Where, I_s, I_r and $\Delta\varphi_m$ are the intensity in sensing arm, intensity in reference arm and phase change due to measurand respectively.

Phase change due to measurand is given as:

$$\Delta\varphi_m = \frac{2\pi}{\lambda_0} L_{int} \Delta N_{eff}$$

where $\lambda_0, L_{int}\ and\ \Delta N_{eff}$ are the wavelength of monochromatic source, interaction length in sensing arm and effective refractive index change due to analyte, respectively.

2.2.3 Sensitive layer

The sensitive layer is the layer which is deposited on the sensing window of the Mach-Zehnder interferometer. It should have transparency, high affinity towards analyte and high refractive index to get high percentage of mode overlap in sensitive layer.

In methane sensing application, cryptophane-A molecule is used as a sensing material. Cryptophane-A is a supramolecule, which has cage like structure. The volume of the host cavity of cryptophane-A is comparable to volume of methane molecule. So, the cavity of cryptophane-A traps the methane molecules when it is exposed to methane gas. Cryptophane-A molecule can also capture chlorofluorocarbon, radon, and xenon. The affinity of other gas has to be further investigated but it is out of scope of this thesis.

Cryptophane-A is a white powder so it requires a host material, which can provide transparency to the layer of cryptophane-A. Styrene acrylonitrile (SAN) polymer is used as a host polymer for cryptophane-A to provide transparency to the cryptophane-A layer. SAN polymer is used because it has high refractive index and has good compatibility with solvent which is used to dissolve cryptophane-A.

2.3 Coupling Techniques:

To make use of a waveguide device, external light must be coupled into the waveguide. To couple light into the waveguide lens coupling, butt-coupling, prism coupling and grating coupling techniques are used. Every coupling technique has its advantages and disadvantages. The coupling efficiency is the most important parameter when comparing the coupling techniques.

We are only using lens coupling and butt-coupling in sensing project. These methods are described in the following sections.

2.3.1 Lens coupling

The lens coupling technique is the most common way of coupling light into the optical waveguide. In this technique, the objective lens is used to focus light on the edge of waveguide to couple light, as shown in Fig 2.5.

The lens coupling is useful for coupling Gaussian laser source to the single mode waveguide because waveguide mode also resembles a Gaussian profile. The coupling efficiency of lens coupling is given as the ratio of overlap integral of incident beam and waveguide mode to the intensity distributions of incident beam and waveguide mode. So, the efficiency can be increased by making the beam spot comparable to the waveguide dimension, so that overlap

between incident beam and waveguide mode is maximum. Mostly, the efficiency of coupling is affected by mismatch in beam spot and waveguide dimension [16].

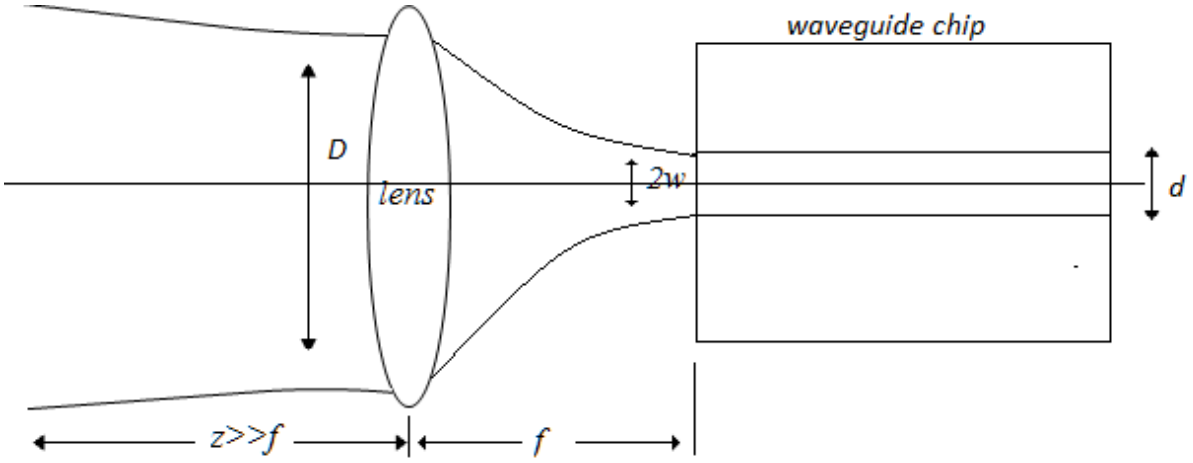

Fig. 2.5 Free space coupling of gaussian beam using lens into waveguide with d,2w, D, f as waveguide thickness, focused beam spot, Beam diameter before lens, and focal length of lens respectively.

The lens coupling is commonly used in laboratory because lens set-up is easy to build and optical bench in laboratory makes it very stable.

2.3.2 Fiber-butt coupling

In this technique, the cleaved end of optical fiber is placed in contact with the end-face of a waveguide to couple light into waveguide. The efficiency of this technique is defined as the ratio of overlap integral of input fiber mode and the waveguide mode, to the fiber and waveguide mode. In order to get higher efficiency, the fiber mode diameter must match with the waveguide mode. Typically, the fiber mode diameter varies in the range of few micrometers for e.g. 5.3 ± 1.0 µm @ 850 nm for PM780-HP, which can give high efficiency if waveguide mode is also in the range of few micrometer. But in our experiment, the dimension mismatch between fiber and waveguide is very high because we use 150 nm thin waveguide, the coupling is very low.

In addition, the immersion oil with same refractive index can be used to reduce losses during coupling because when light travels from one refractive index medium to other, light undergoes refraction if air is present between both materials and it is lost.

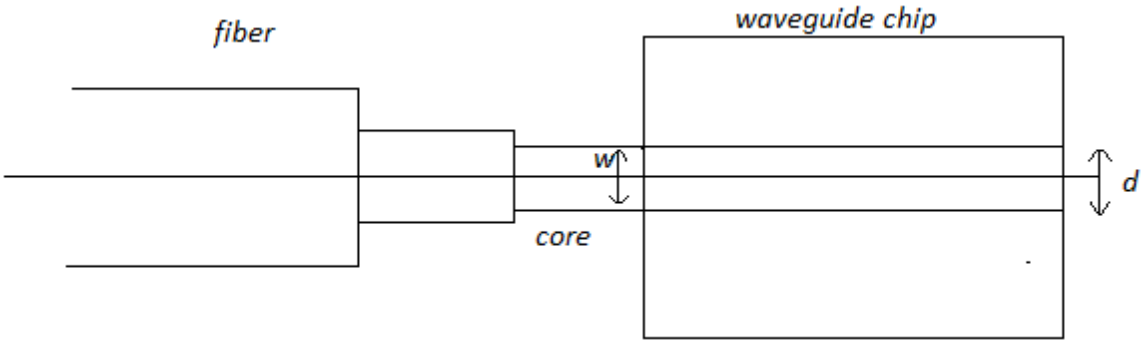

Fig. 2.6 Butt-coupling

Butt-coupling is commonly used in place of lens coupling because it provides much better mechanical stability to the set-up. And in butt-coupling, the fiber can be strongly glued (fiber-pigtailing) with waveguide that makes it more useful in industrial application.

Chapter 3

Experimental set-up and chip processing

3.1 Chip Design

When I started my master thesis, the waveguide chip for the methane sensor was already designed and fabricated. It was designed by Dr. Firehun Tsige Dullo, Dr. Susan Lindecrantz and Prof. Olav Gaute Hellesø. I have included this section to explain the background of the waveguide chip design.

The waveguide chips are designed using CleWin 5 (Phoenix). The dimension of each waveguide chip is 25x40x1 mm^3. Each waveguide chip has many Mach-Zehnder interferometers, Young interferometers and straight waveguides. The waveguides are shallow rib waveguides with a silicon nitride core. The dimensions of the waveguide are chosen after precise simulations for single mode for both TE and TM polarization and for 785 nm wavelength. The silicon Nitride core has a thickness of 150 nm over a silica layer. The rib height is 5 nm. The rib waveguide is chosen because it gives low propagation loss [11]. The waveguides are top cladded with silica of 1 µm thickness. The Y-junction for the Mach-Zehnder interferometers are designed with S bends with a radius of 4 mm. The sensing arm of each Mach-Zehnder interferometer are opened with a width of 25 µm in the silica layer to create sensing window. The Mach-Zehnder interferometers are designed for 3 waveguide widths (1.5 µm, 2 µm, 3 µm). For each waveguide width, 3 different lengths (1 cm, 2 cm, and 3 cm) of sensing windows are designed. Along with unbalanced Mach-Zehnder interferometers with sensing window on one arm, some balanced Mach-Zehnder interferometers are also designed with sensing window on both arms with a center to center distance of 50 µm. The waveguides are fabricated at IMB-CNM, CSIC, Barcelona, Spain [18].

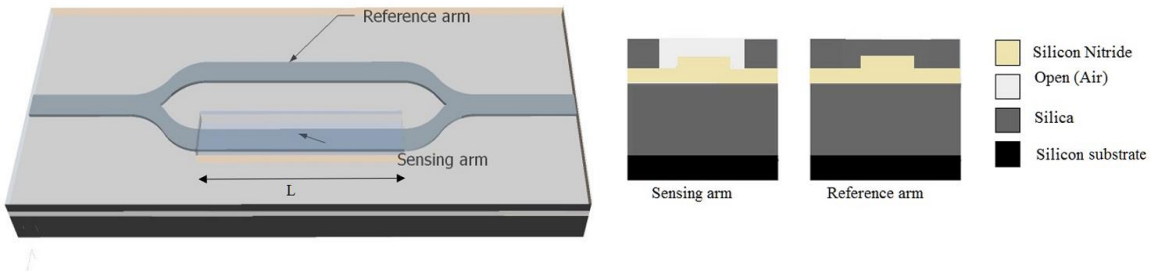

Fig 3.1 Schematic diagram of Mach-Zehnder interferometer with 1 sensing window with sensing length L.

3.2 Experimental Set-up

Experimental set-up for methane sensing broadly be divided into two parts, the optical set-up and the gas flow set-up.

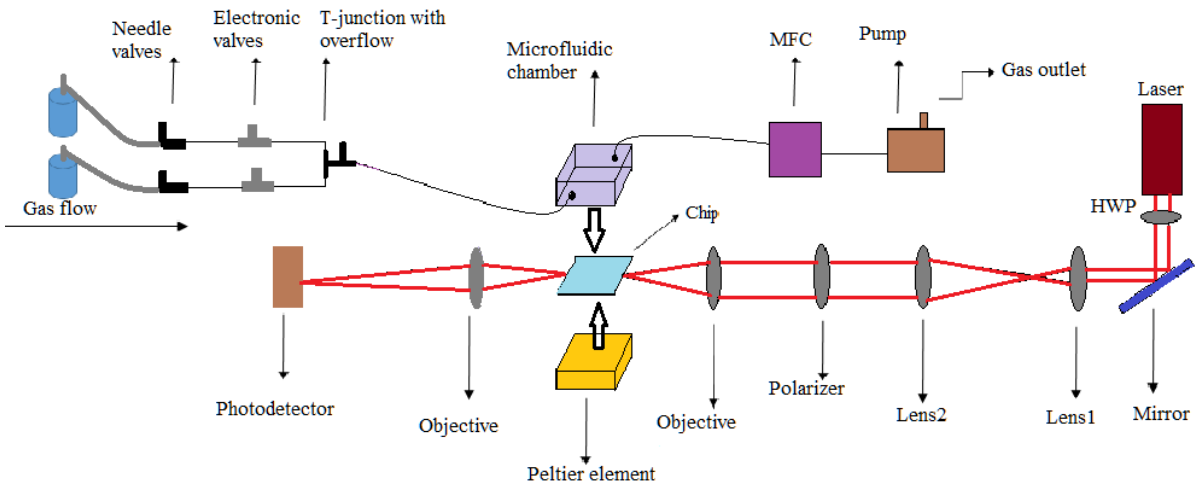

Fig. 3.2 Schematic diagram of experimental set-up

3.2.1 Optical set-up

In the optical set-up, the collimated solid state laser source of 785 nm wavelength was used (DL785-120-SO, CrystaLaser, USA). The half wave plate was placed in front of the laser source to adjust the polarization. A mirror was used at 45^o to reflect light in the desired direction. Then, two lens were placed at a distance of f_1+f_2 from each other to expand beam and adapt it to the microscope objective. The beam was passed through a linear polarizer to

select polarization (TM) and finally beam was collected by input objective lens (25x) to focus light on the input facet of the waveguide for coupling. The input objective was placed on the 3-axis piezo controller, which was used to adjust the focus on the input facet of chip. After chip, light was collected by the 10x output objective, which focusses the collected light into the photodetector. Absorptive neutral density filter was also placed between output objective lens and the photodetector to control the output power to match power range of photodetector.

During my thesis work, I used the existing optical set-up.

3.2.2 Gas flow system

The layout of the gas flow set-up is shown in Fig. 3.2. Two calibrated gas bottles of nitrogen and methane (1000 ppm) were used. During the measurement, the output pressure of bottles was fixed at 2 bar. Two electronic valves (Parker VAC-100 PSIG) in a T-junction were used to electronically control the switching of gas between nitrogen and methane, the valves were controlled by LabVIEW. But, valves were resulting in waste of gas when closed because gas from bottles were directly coming to the valves with very high flow rate. To avoid that, needle valves were placed before the electronic valves to reduce the flow rate of the gas and regulate the flow during the measurement. An overflow was included in a T-junction to regulate the flow rate of the gas going into the microfluidic chamber and to perform the measurement at atmospheric pressure. At output, one pump was placed, which was required to create pressure difference for continuous flow of gas. In addition, one MFC was placed before pump, which was working as a flowmeter.

3.2.3 Chip holder and microfluidic chamber

A 1-dimensional translation stage was used to hold the waveguide chip as shown in Fig 3.3 (a). The peltier element was fixed on the translational stage to regulate the temperature of chip. Above peltier element, the aluminium plate was placed with a thermal paste to provide better thermal conductivity. The aluminium plate was designed with grooves to hold the chip and a thermistor was fixed in aluminium plate to provide feedback to temperature controller.

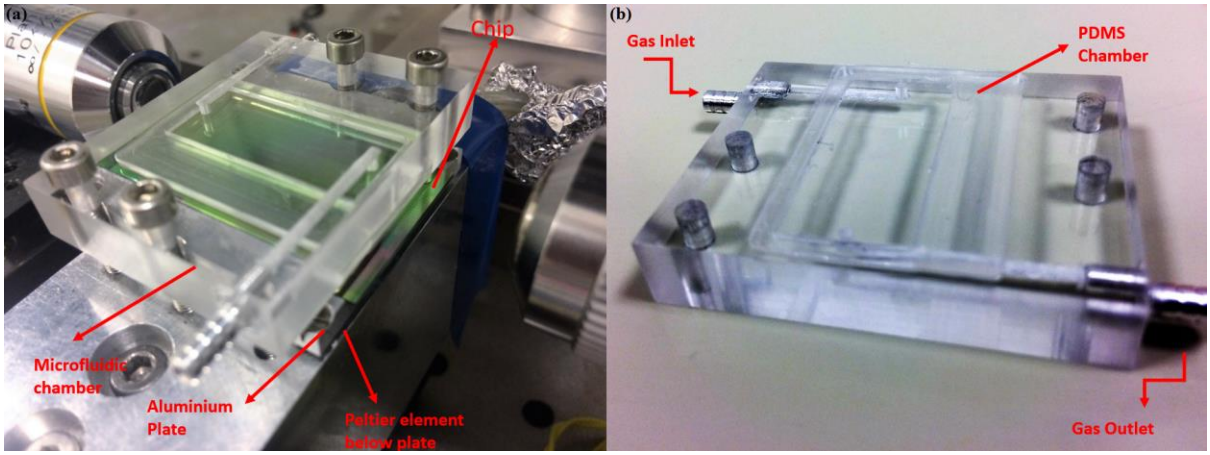

Fig 3.3 (a) set-up for chip placement, (b) Microfluidic chamber

The microfluidic chamber was placed above waveguide chip. The microfluidic chamber was fabricated with rectangular grooves, which was used to place PDMS chamber, which provides the air tight flow of gas through chip as shown in Fig 3.3 (b).

3.3 Chip processing

To make waveguide chip sensitive towards methane, deposition of SAN doped with cryptophane-A polymer layer on sensing window of Mach-Zehnder interferometer was required.

To deposit the sensitive layer on Silicon Nitride surface, surface cleaning, surface activation and salinization process was required to get adhesive surface for sensitive layer. The protocol for cleaning and salinization is described in next section.

3.3.1 Chip cleaning/recycling protocol

A cleaning procedure was followed when chip was not used for long time and has acquired dust. First, the chip was cleaned with clean-room swap soaked in Acetone. Then, the chip was sonicated for 5 minutes with Acetone, isopropanol and distilled water successively. The chip was then dried with nitrogen and introduced in the hellmenax (5%) solution for 10 minutes at 70 °C. After hellmanex, the chip was thoroughly rinsed with distilled water to remove residuals of hellmanex and dried with nitrogen.

If the chip had been processed before with sensitive layer, then it required a recycling process to make it reusable again. For, recycling, first step was to dip the chip in dynasolve solution for half an hour to remove PDMS (if chip was processed with PDMS before). Then, the chip

was cleaned with the similar procedure which is described before. After cleaning procedure, the chip was sonicated with 1:1 solution of HCl (37%) and Methanol for 10 min, rinsed with distilled water and dried with nitrogen. The chip was then introduced in the air plasma for 10 minutes, rinsed with isopropanol, distilled water and finally dried with nitrogen.

3.3.2 Surface activation and silanization of chip

Before deposition of sensitive polymer layer on the chip, the silanization process was required which provides the better adhesion between deposited layer and the chip. It was an important step for our sensing application as we deposit sensing polymer layer on silicon nitride chip, which has a very hard and smooth surface.

For silanization, the recycled chip was first placed in air plasma for half an hour to activate the chip surface. Then, the chip was immersed in 1% of (3-Aminopropyl) triethoxysilane (APTES) solution for 1 hour at 40°C. The chip was then rinsed with isopropanol (or ethanol) and cured in oven for 1 hour at 110 °C.

The APTES (1%) was prepared by heating the mixture of 20 ml ethanol (96%) with 0.2 ml APTES at 40 °C for 1 hour.

3.3.3 Preparation of sensitive layer and deposition

For methane sensing, a layer of SAN doped with cryptophane-A was required to be deposited on the sensing window of the Mach-Zehnder interferometer.

To deposit 300 nm-400 nm thick layer of SAN doped with 11% cryptophane-A. First the 5 mg of cryptophane-A was measured and then added to 900 µl of 1,1,2,2 Tetrachloroethane solution kept in a vial. The solution was slowly mixed for 10 minutes and then 45 mg of SAN was added to that solution. Solution was then kept overnight to get uniformly mixed. The uniformly mixed solution was then spin coated on the chip (directly after silanization of the chip) with speed of 3000 rpm for 2 minutes. For curing, the chip was placed overnight in an oven at 110°C. And the thickness of SAN doped with cryptophane-A layer was measured with a stylus profiler (KLA-Tencor P-6).

In order to deposit the different thicknesses of SAN doped with cryptophane-A on the chip. The dependence of thickness of sensitive layer with the volume of solvent (1, 1, 2, 2 Tetrachloroethane) was investigated. First, the investigation was done for the pure SAN polymer. The measured thickness of SAN polymer layer with change in the volume of solvent is listed in Table.3.1. From the measured thicknesses of the SAN polymer, we found that the

thickness decreases with increase in the volume of solvent. In order to understand the relation of thickness with solvent volume, thicknesses for different concentrations of SAN is plotted in Fig. 3.4. The change in thickness shows approximately a linear trend with concentration of SAN solution.

Table 3.1 Thickness vs SAN concentration

Amount of SAN (mg)	Volume of solvent (µl)	SAN solution concentration (g/ml)	Spin coating speed (rpm)	Thickness (nm)
49.5	900	0.055	3500	375
51	1800	0.028	3500	147
48.4	2700	0.018	3500	83

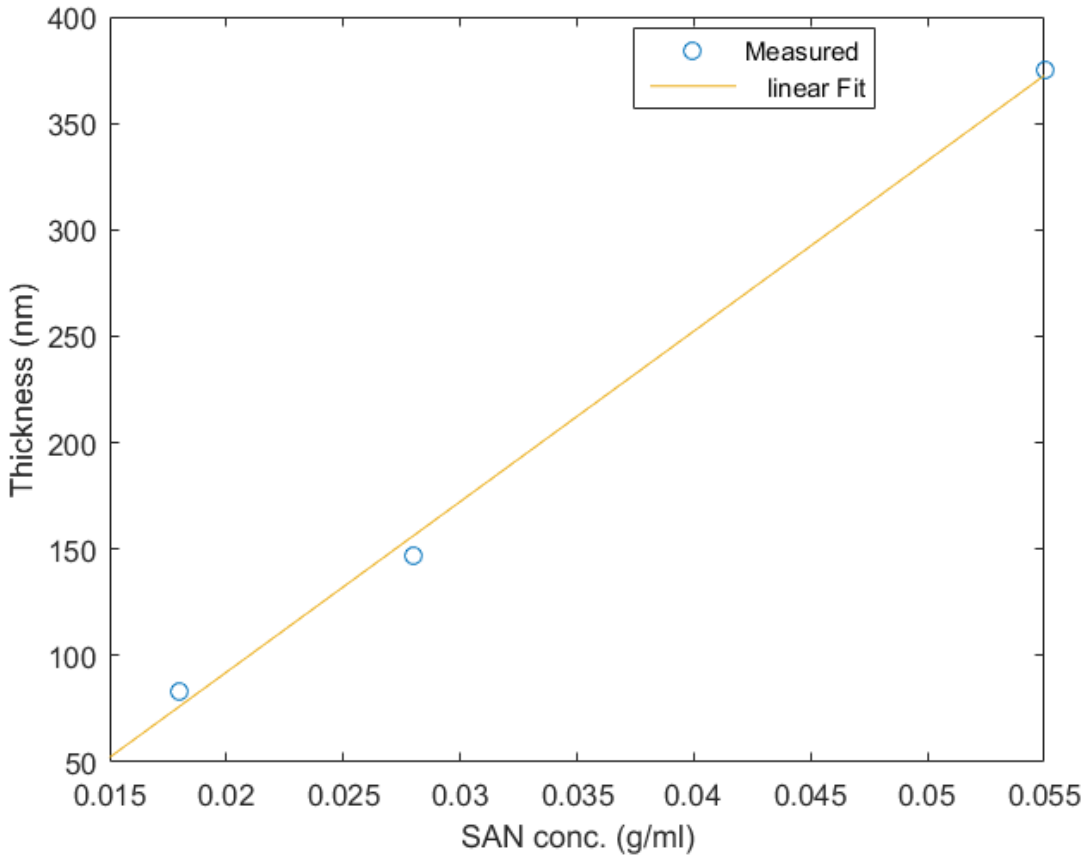

Fig 3.4 SAN Concentration Vs Thickness

After, estimation of linear behavior of thickness of SAN with solvent. We expected the same behavior with doped SAN. Then the same procedure was followed with SAN doped with 11% cryptophane-A. The solution was prepared with the same ratio as shown in Table 3.1. We

replaced the 50 mg of SAN with 45 mg of SAN added with 5 mg cryptophane-A. But the measured thickness was not as expected from Fig.3.5. From the measurement of thickness, we found that the solubility of cryptophane-A in the solvent was high in comparison to SAN polymer which resulted in completely different thickness. So, we decided to consider only the amount of SAN polymer for estimation of different thicknesses. The measurement results for thickness of SAN doped with 11% cryptophane-A with volume of solvent is listed in Table. 3.2. The measured results were giving good match with measured results for pure SAN.

Table 3.2 Thickness vs volume of solvent

Amount of SAN (mg)	Amount of Cryptophane-A (mg)	Volume of solvent (µl)	Spin coating speed (rpm)	Thickness (nm)
44.8	5.5	700	3500	560
44.6	5.2	900	3500	375
44.6	5.2	150 +450 (above solution)	3500	257
42.5	5.6	1800	3500	137

During all the depositions, the recycling, silanization and the curing process were followed as described in section 3.3.2.

The sensitive layer deposition process described in the section was used to deposit the sensitive layer on the unbalanced Mach-Zehnder interferometer because during the spin coating, the sensitive layer covers the whole chip. So, the balanced Mach-Zehnder interferometers which were fabricated on the chip with 2 sensing windows were also completely covered. The deposition of sensitive layer on both arms of balanced Mach-Zehnder interferometer makes the sensor insensitive to methane, which is discussed in detail in chapter 4 and 6. In order to develop the sensor with balanced Mach-Zehnder interferometer, the further processing of the chip is presented in next section.

3.3.3.1 Photolithography

The photolithography process was chosen to perform the processing of balanced Mach-Zehnder interferometer, because photolithography is commonly used in microfabrication to pattern thin layer substrate and our requirement was also to pattern 25 µm wide open sensing window. We used photolithographic process to pattern the thin layer of silver on one arm of

the balanced Mach-Zehnder interferometer to reduce the temperature sensitivity which is evident in unbalanced Mach-Zehnder interferometer which has silica in one arm (chapter 4,6).

To start with photolithographic process, we started with optimization of exposure time and development time for the available photoresist. After, optimization we started working on deposition of silver on one arm of the balanced Mach-Zehnder interferometer.

To deposit silver in one arm. First, we deposited the 351 nm thick sensitive layer of SAN doped with 33% cryptophane-A on the chip by following the same procedure as described in section 3.3.3. Then, on the top of sensitive layer a 120 nm thin layer of silver was deposited using sputtering machine (Aja Orion-5). After deposition of silver layer, a layer of SPR-700 I (positive) was deposited. Then, the chip was kept at room temperature for 30 min, the pre-bake process was avoided to prevent expansion of polymer which was causing cracks in silver layer. After drying, MJB4 Mask-Aligner was used to align the mask to expose one arm of the balanced Mach-Zehnder interferometer. After alignment, the chip was exposed with 200 mJ intensity. Then, photoresist was developed in NaOH solution (2 gm NaOH + 300 ml water) for 5-10 seconds. After, development of photoresist, the chip was dipped in silver etchant (20 gm Ferric Nitrate +40 ml water) for 10-15 sec to etch out the silver from exposed region.

But we found that the silver was also etching out from the unexposed region. We tried this many times, but every time the silver was etching out from unexposed region also. The possible reasons for this can be the use of SPR 700 I which gives very thin layer, the use of NaOH (which is commonly not preferred) and pre-bake (post-bake) was also avoided during the processing.

Then we decided to work with Negative photoresist (651796 ALDRICH), developer (651788) and remover (651761), but we found out that the photoresist and developer were attacking the SAN polymer.

From all followed procedures, we found that the available photoresist kits are not compatible with SAN polymer. Then, we decided to work with Microplotter, which was available in ultrasound lab.

3.3.3.2 Microplotter

The Microplotter II is a dispenser which uses ultrasonics to deposit fluid on a surface. This can produce picolitre droplets that can deposit 5 micron wide patterns. For deposition of pattern, micropipette is connected to an inbuilt robot. The inbuilt robot can move in all the 3 directions. The droplet size and deposition speed of robot is controlled by sonoguide software. In addition, to track the deposition, a high-resolution camera is connected to the robot. We used Microplotter to deposit SAN in one and SAN doped cryptophane-A in other arm of the

balanced interferometer, to make the sensor with high. For deposition SAN and doped SAN, we assumed that the thermo-optical coefficient is same for both pure SAN and doped SAN, because same thermo-optical coefficient makes the sensor insensitive (discussed in detail in chapter 6).

The Mach-Zehnder interferometer chosen for this deposition were from new batch of chips because the sensing window in new Mach-Zehnder interferometers were 100 µm wide and the center to center distance between two sensing windows were 125 µm. That makes the deposition easy in comparison to old chip, which had only 50 µm gap between both arms. The Mach-Zehnder interferometers in the new chip were designed and fabricated by same process as mentioned in section 3.1. The difference between old and new chips were the sensing window length (0.5 cm and 2.5 cm).

To deposit SAN in one arm and doped SAN in other. First, we started with deposition of pure SAN on both arms. Before deposition, the chip was silanized for better adhesion. Then, pure SAN solution was filled in the micropipette (10 µm). Then using that micropipette, pure SAN was plotted on the both arms of the balanced Mach-Zehnder interferometer (0.5 cm long sensing window). And after plotting it was cured overnight at 110 °C.

After curing, the laser was coupled into the waveguide to test the losses in the sensing window. The waveguide was found to be very lossy, a lot of scattering points were present in the sensing windows. The possible reasons can be the adhesion problem, formation of bubble during plotting and dirt.

In order to remove possible causes of scattering, a thin layer (80nm) of pure SAN was deposited on the chip, using spin coater. Then, chip was cured for 2 hours. After curing, 400 nm thick layer of pure SAN and SAN doped with 25% cryptophane-A were plotted on both arms of the balanced Mach-Zehnder interferometer (0.5 cm long sensing window length). After deposition chip was cured overnight at 110 °C. When the light was coupled into the waveguide, there were no scattering points. Then it was used for methane, measurement results are presented in Chapter 6.

3.4 Refractive index measurement

In order to do simulations (discussed in chapter 4 and 5), the refractive index measurement was done for pure SAN and SAN doped with different concentrations of cryptophane-A. Refractive index measurement was done with prism coupler. For measurement of refractive index, thick layer (700-1000 nm) of SAN and doped SAN were deposited on silica chips. The thick layer was deposited to get atleast two waveguide modes, because prism coupler requires two waveguide modes to measure refractive and film thickness precisely. The measured refractive index are listed in Table. 3.3.

Table 3.3. Measured Refractive index of sensitive layer

Sensitive layer	Refractive index
Pure SAN	1.5588±0.0042
SAN doped with 11% cryptophane-A	1.5634±0.0022
SAN doped with 50% cryptophane-A	1.5821±0.0018

From measurement of refractive index, we found that the refractive index was increasing with increase of doping with cryptophane-A.

Chapter 4

Measurement of sensitivity and Response time

4.1 Sensitivity

The theoretical background of methane sensitivity of the Mach-Zehnder interferometer is discussed in this section. A change of refractive index or path length in the sensing arm of the interferometer results in a phase change at the output. In our case, this phase change is due to refractive index change of the top cladding layer if methane concentration in the surrounding environment changes. This change is enhanced by deposition of a sensitive layer, which has affinity towards methane. The phase change at the output relative to methane concentration gives the sensitivity of the sensor.

4.1.1 Phase sensitivity

When monochromatic light with wavelength λ_0 is coupled into a waveguide, continuity of the tangential components results in an evanescent field in the cladding regions. The extension of the evanescent field depends on the waveguide geometry and the index contrast between the core and the top and bottom cladding. A change in refractive index of the cladding results in a change in the effective index of the guided mode, which results in a phase change at the end of the waveguide.

The phase at the output of a waveguide (φ_1) is given as:

$$\varphi_1 = \frac{2\pi}{\lambda_0} L n_{eff} \qquad 4.1$$

where L is the length of the waveguide and n_{eff} is the effective index of the guided mode. Any change in L or n_{eff} results in a change of phase at the end of the waveguide. Small change in physical and chemical quantities can affect n_{eff}.

For fixed waveguide length, the phase change due to physical (temperature, pressure) and chemical (methane) parameters can be given as:

$$\frac{\partial \varphi_1}{\partial A} = \frac{2\pi}{\lambda_0} L_{int} \frac{\partial n_{eff1}}{\partial A} \quad 4.2$$

This equation can also be written as:

$$\frac{\partial \varphi_1}{\partial A} = \frac{2\pi}{\lambda_0} L_{int} \frac{\partial n_{eff1}}{\partial n_1} \frac{\partial n_1}{\partial A} \quad 4.3$$

where n_1 is the refractive index of the cover (top cladding) on the arm, n_{eff1} is the effective index of the guided mode in the arm and A is the physical/chemical parameter which changes the index of the cover.

Similarly, for the other arm of the interferometer, the phase change at the end of the arm can be given as:

$$\frac{\partial \varphi_2}{\partial A} = \frac{2\pi}{\lambda_0} L_{int} \frac{\partial n_{eff2}}{\partial A} = \frac{2\pi}{\lambda_0} L_{int} \frac{\partial n_{eff2}}{\partial n_2} \frac{\partial n_2}{\partial A} \quad 4.4$$

where n_2 is the refractive index of the cover (top cladding) on the other arm and n_{eff2} is the effective index of the guided mode.

From eq. 4.3 and 4.4, the phase sensitivity of the interferometer to the parameter A, $\frac{\partial \varphi_m}{\partial A}$, can be calculated, and is defined as the relative phase change between the arms for a specific analyte or physical parameter change.

$$\frac{\partial \varphi_m}{\partial A} = \frac{\partial \varphi_1}{\partial A} - \frac{\partial \varphi_2}{\partial A} = \frac{2\pi}{\lambda_0} L_{int} \frac{\partial n_{eff1}}{\partial n_1} \frac{\partial n_1}{\partial A} - \frac{2\pi}{\lambda_0} L_{int} \frac{\partial n_{eff2}}{\partial n_2} \frac{\partial n_2}{\partial A}$$

$$\frac{\partial \varphi_m}{\partial A} = \frac{2\pi}{\lambda_0} L_{int} \{ \frac{\partial n_{eff1}}{\partial n_1} \frac{\partial n_1}{\partial A} - \frac{\partial n_{eff2}}{\partial n_2} \frac{\partial n_2}{\partial A} \} \quad 4.5$$

Where $\frac{\partial \varphi_m}{\partial A}$ is the phase sensitivity for parameter A.

4.1.2 Methane sensitivity

For methane sensing, a Mach-Zehnder interferometer with one Sensing window (SW) was used (Fig. 3.1). The reference arm was cladded with silica and the sensing arm was cladded with a sensitive polymer layer. From eq. 4.5, the phase sensitivity to methane with concentration x can be calculated as:

$$\frac{\partial \varphi_m}{\partial x} = \frac{2\pi}{\lambda_0} L_{int}\{\frac{\partial n_{eff1}}{\partial n_1}\frac{\partial n_1}{\partial x} - \frac{\partial n_{eff2}}{\partial n_2}\frac{\partial n_2}{\partial x}\} = \frac{2\pi}{\lambda_0} L_{int}\{\frac{\partial n_{eff1}}{\partial n_1}\frac{\partial n_1}{\partial x}\} \quad 4.6$$

where the second term becomes zero as the silica is impermeable to methane and thus the change in refractive of silica with methane concentration is equal to zero ($\frac{\partial n_2}{\partial x} = 0$).

The sensitivity to methane depends on the input wavelength (λ_0), the length of the sensing arm (interaction length, L_{int}), the change in refractive index of the sensitive layer with methane concentration ($\frac{\partial n_1}{\partial x}$), and the effective index change due to change in refractive index of the cladding ($\frac{\partial n_{eff1}}{\partial n_1}$). For fixed interaction length and wavelength, the methane sensitivity is dependent on the product of the last two terms, which are discussed in separate sections below.

4.1.2.1 Sensitivity due to cladding refractive index and thickness

To investigate the effect of change in refractive index and thickness of the cladding on the sensitivity, simulations using Fimmwave (PhotonDesign) were carried out by Dr. Jana Jágerská. The change in effective refractive index resulting from a small change in refractive index of the cladding were simulated for 4 different refractive indices of the cladding corresponding to the refractive indices of pure SAN (n=1.5588) and SAN doped with 11% (n=1.5634), 33% (n=1.5733), and 50% (n=1.5821) cryptophane-A. The refractive indices of SAN and cryptophane-A doped SAN were determined experimentally using prism coupler as described in section 3.4.

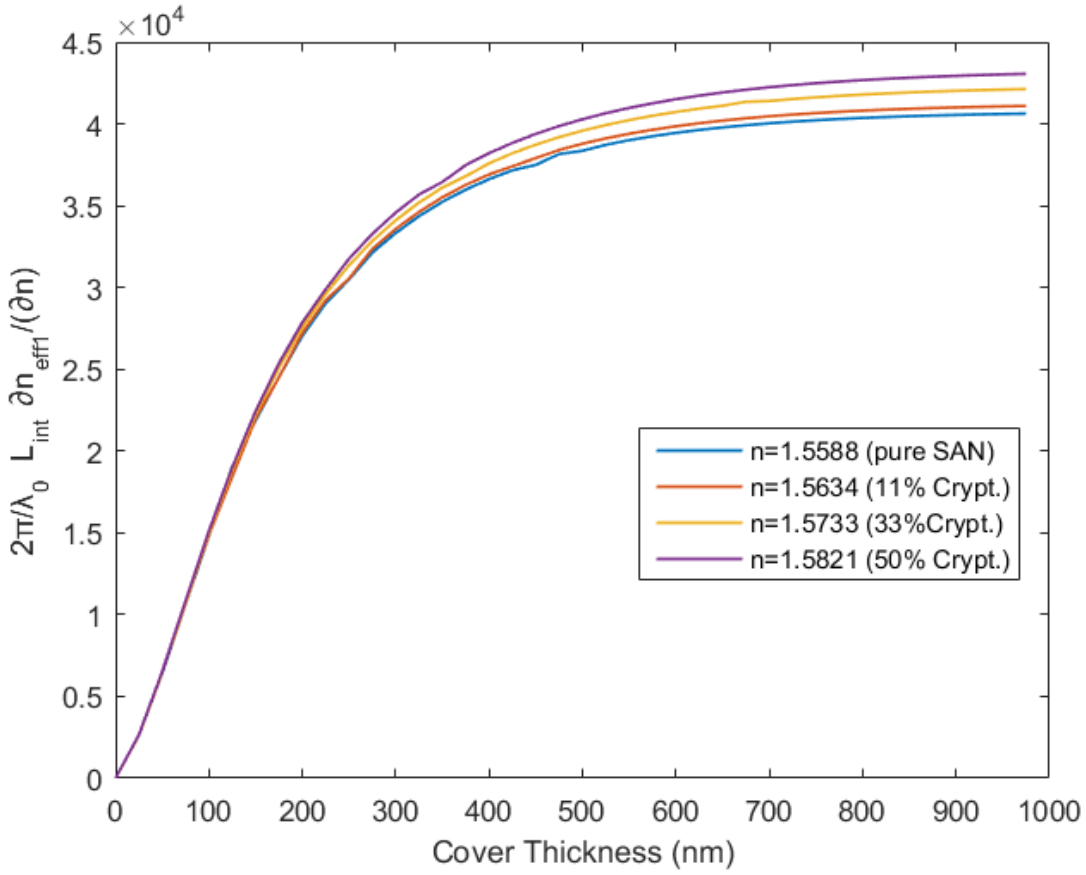

Fig 4.1 Sensitivity vs cover thickness

As shown in Fig. 4.1, the simulation results show that the sensitivity increases with increasing thickness of the cladding, before it gets saturated at a certain thickness of the cladding. With increase in the refractive index of the cladding, the saturation level increases slightly. The simulation results show that to attain high sensitivity, the refractive index of the cladding should be high and its thickness must be approximately 500 nm, corresponding to the extent of the evanescent field.

4.1.2.2 Sensitivity due to methane concentration

The factor $\frac{\partial n_1}{\partial x}$ in eq. 4.6 describes the sensitivity towards methane.

For methane sensing, SAN polymer was doped with cryptophane-A and used as the cladding in the sensing window (see section 2.2.3). The methane sensitivity for both pure and doped SAN polymer is described in this section.

4.1.2.2.1 Styrene acrylonitrile (SAN)

The refractive index change of SAN in the presence of methane is discussed in detail in the thesis of Martin Ingvaldsen [24]. The refractive index change in SAN with methane gas is assumed as the function of solubility of methane and the methane concentration. From Henry's law, the solubility of a gas in a polymer is directly proportional to the partial pressure of the gas in the equilibirium with polymer [28].

The refractive index $n_1$of SAN with methane of concentration x (in nitrogen) can be given as [24]:

$$n_1 - 1 = n_{SAN} - 1 + (n_{N_2} - 1)C_1(1 - x) + (n_{N_{CH4}} - 1)C_2 x \quad 4.7$$

where n_{N_2} is the refractive index of nitrogen, $n_{N_{CH4}}$is the refractive index of methane, $n_{SAN}$is the refractive index of pure SAN, C_1 is the solubility of nitrogen in pure SAN, and C_2 is the solubility of methane in pure SAN.

The refractive indices of methane and nitrogen are 1.000437 and 1.000268, respectively [24].

Then, the sensitivity of methane for methane concentration can be calculated as:

$$\frac{dn_1}{dx} = n_{CH_4}C_2 - n_{N_2}C_1 = 0.000437C_2 - 0.000268C_1 \quad 4.8$$

The solubility of the methane and nitrogen in SAN polymer were not found in literature, however, based on solubility values in other polymers we can assume that the C_1 and C_2 are close to unity. Under this assumption, the sensitivity is 1.7 x 10^{-5} refractive index change per ppm.

4.1.2.2.2 Sensitivity enhancement with cryptophane-A

The pure SAN polymer was doped with cryptophane-A to enhance the sensitivity of methane as the cryptophane-A has high affinity towards methane (see section 2.2.3). As described in section 2.2.3, the cryptophane-A traps methane molecules in its host cavity. So, the refractive index $n_1$of SAN doped with cryptophane-A in the presence of methane of concentration *x* (in nitrogen) can be given as [24]:

$$n_1 - 1 = n_{SAN+Crypt} - 1 + (n_{N_2} - 1)C_3(1 - x) + (n_{CH_4} - 1)C_4 x + f_{trap}(x, c) \quad 4.9$$

Which can be written as:

$$n_1 - 1 = n_{SAN+Crypt} - 1 + (0.000268)C_3(1-x) + (0.000437)C_4 x + f_{trap}(x,c) \quad 4.10$$

where, $f_{trap}$is the refractive index due to trapped methane which depends on the concentration of cryptophane-A (c) and the concentration of methane (x), $n_{SAN+Crypt}$is the refractive index of cryptophane-A doped SAN polymer, n_1 is the refractive index of cryptophane-A doped SAN with methane which includes both trapped and dissolved methane, C_3 is the solubility of nitrogen in cryptophane-A doped SAN, and C_4 is the solubility of methane in cryptophane-A doped SAN.

Then, the sensitivity for methane concentration can be given as:

$$\frac{dn_1}{dx} = 0.000437C_4 - 0.000268C_3 + \frac{\partial f_{trap}(x,c)}{\partial x} \quad 4.11$$

Our group has previously reported that the enhancement factor (pre-concentration) is linearly dependent on the concentration of methane [22]. Therefore, eq. 4.18 can be written as:

$$\frac{dn_1}{dx} = 0.000437C_4 - 0.000268C_3 + f_{trap}(c) \quad 4.12$$

4.2 Experimental analysis of sensitivity

4.2.1 Experimental method

This section describes the experimental procedure for the measurement of the methane sensitivity. To experimentally measure the concentration of methane, calibrated mixture of 0 and 1000 ppm methane in nitrogen was alternatively introduced into the microfluidic chamber of the chip. A TM polarized laser beam of 785 nm wavelength was coupled into a Mach-Zehnder interferometer. A Mach-Zehnder interferometer with 2 μm wide waveguide and 3 cm long sensing window (interaction length) was used.

In Fig 4.2(b), the sensor response, i.e. output intensity, is shown when methane concentration was alternatively changing between 0 and 1000 ppm. The response is reproducible and repeatable for alternate switching of methane and nitrogen. The phase change, as shown in Fig 4.2(c), was calculated as:

$$\Delta\varphi(t) = \Delta\varphi_0 + arccos((I_{meas}(t) - (I_S + I_r))/2\sqrt{I_r I_s}) \quad 4.13$$

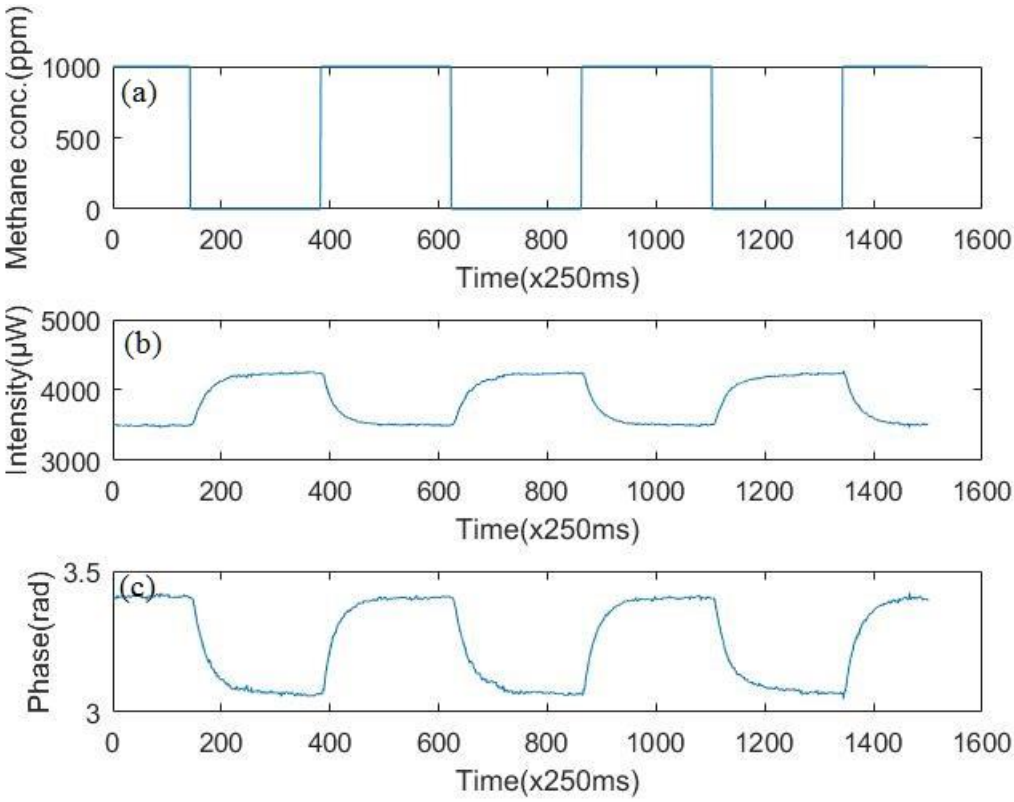

Fig 4.2 (a) Input methane concentration, (b) Intensity change at output due to varying methane concentration, (c) Phase change at output. The measurement was done for 10.5% concentration of cryptophane-A

where I_S is the intensity in the sensing arm, $I_r$is the intensity in the reference arm, $\Delta\varphi_0$is the initial phase shift between both arms and $\Delta\varphi(t)$ is the output phase change.

Experimentally, I_S and I_r were calculated from I_{max} and I_{min} of output intensity as $I_S + I_r = {(I_{max} + I_{min})}/{2}$ and $2\sqrt{I_r I_S} = {(I_{max} - I_{min})}/{2}$.

In the following analysis, sensitivity was calculated as S=$\frac{\Delta\varphi}{\Delta x}$, where Δx (1000 ppm) is the concentration of methane used in experiments. The response time of the sensor was taken as the rise time from 10% to 90% of total phase change.

4.2.2 Measurement results for higher sensitivity

As mentioned in section 4.1.2.2.2 and [22], the sensitivity increases with the cryptophane-A concentration in SAN. In this section, measurements with different cryptophane-A concentration are presented for a fixed thickness of the sensitive layer of about 350 nm. The

measurement results are listed in Table 4.1. First the sensitivity measurement was done for 10.5% cryptophane-A in SAN. This measurement was done primarily to compare the measured sensitivity with the previously reported sensitivity [22]. The measured sensitivity 0.42 x 10^{-3}rad/ppm was found to be slightly higher than the previously reported 0.29 x 10^{-3}rad/ppm. A possible explanation for this is that in the previous measurement the thickness was smaller, around 220-250 nm. Another possible reason is that different batches of cryptophane-A of different purity were used. The measured sensitivity for 33% cryptophane-A was found to be more than double in comparison to 10.5 %.

Table 4.1 Measurement results for different concentrations of cryptophane-A

Concentration of cryptophane-A (%)	Thickness (nm)	Sensitivity(x10^{-3})	Response time (s)
10.5	375	0.417	22.5
33	351	0.89	66

To find the maximum sensitivity, the concentration of cryptophane-A was further increased. For this measurement, a thick (538 nm) layer of SAN doped with 50% cryptophane-A was deposited. From the measurement result shown in Table 4.2, the sensitivity was found to be almost twice the sensitivity for 33 %, i.e. 1.71 x 10^{-3}rad/ppm.

Further increase of cryptophane-A concentration was attempted (67%), however, the scattering of light in the sensing window became prominent and the visibility of the interference fringes was very low. It is possible that at the concentration of 67%, cryptophane-A starts clustering in the SAN host upon solvent evaporation. Because of bad visibility and a lot of scattering losses, we considered 50% cryptophane-A the limit giving maximum sensitivity.

Table 4.2 Measurement for maximum sensitivity

Concentration of cryptophane-A (%)	Thickness (nm)	Sensitivity(x10^{-3})	Response time (s)
50	538	1.71	616

These measurements clearly show that the sensitivity is increasing with increase in cryptophane-A concentration, but along with that, the sensor response is getting slow as shown in Table 4.1 and 4.2. So, in order to develop a highly sensitive and fast sensor, a compromise between sensitivity and response time has to be made. Work towards this is presented in next section.

4.2.3 Measurement results for optimum thickness of polymer layer

In this section, both the sensitivity and the response time were measured as a function of the thickness of the cladding. In section 4.1.2.1, the simulation results for sensitivity change with cladding thickness was presented, which show that the sensitivity decreases with decrease in cladding thickness. The response time is also expected to decrease with decrease in cladding thickness because with thin layer, the number of trapping sites for methane is smaller, and the otherwise extremely fast diffusion is not hindered by the effect of trapping. The investigation of response time was motivated by the fact that as the aim of our project is to develop not only sensitive, but also a fast methane sensor with a response time of a few seconds.

For measurement of response time and sensitivity with cladding thickness, measurements with (11±0.5) % cryptophane-A doped SAN were done. The measurement results are listed in Table. 4.3 and shown in Fig. 4.3.

Table 4.3 Measurement data for varying thickness of sensitive layer

Concentration of cryptophane-A (%)	Thickness (nm)	Sensitivity($x10^{-3}$)	Response time (s)
11.6	137	0.1441	3.2
10.5	260	0.3446	14
10.5	375	0.4170	22.5
10.9	560	0.3750	43.5
11±0.5			

The sensitivity increases with thickness before it saturates around 400 nm. The sensitivity change measured was found to be similar to the simulation results as shown in Fig. 4.1.

The response time change with change in the sensing layer thickness follows the assumption of fast response in thin layer. To analyze the response time of the sensor, we assume that the penetration of methane into the sensing layer can be described by the Fick's law of diffusion [26]. The diffusion rate for methane gas in polymer can be written as $\frac{C(x,t_{90})}{C_0} = \mathrm{erf}(\frac{x}{\sqrt{4Dt_{90}}})$, where $C(x,t_{90})$ is the methane concentration at time t_{90} (rise time) for polymer with x thickness, C_0 is initial concentration of methane (outside polymer) and D is the diffusion coefficient. From the above equation, the quadratic relation between thickness and response

time was found. The quadratic function given by Fick's law was fitted with measured data as shown in Fig. 4.3 (b). As shown, the quadratic function can be considered a good fit. The diffusion coefficient found from the fit was 2.4 x 10^5 nm^2/sec.

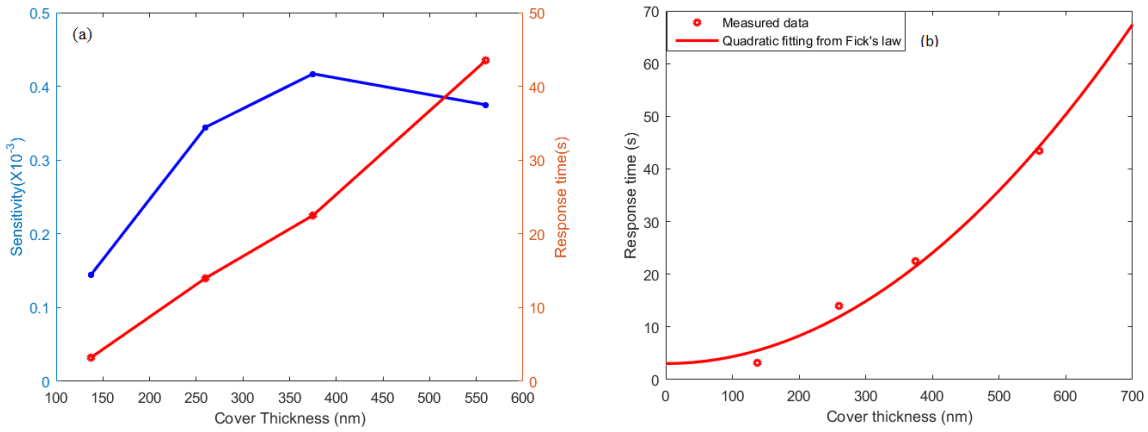

Fig 4.3 Plot of sensitivity and response time vs sensitive layer thickness (11±0.5% cryptophane-A)

From Fig 4.3, the optimum thickness of the sensitive layer can be found for required sensitivity and response time. According to our requirement for fast response time, we have to make a compromise between sensitivity and response time. So, optimum thickness for 11% cryptophane-A doped SAN was chosen to be 150 nm, corresponding to the sensitivity of 0.2 x 10^{-3}rad/ppm and the time response below 5s.

From the measurements with 11 % cryptophane-A doped SAN, it can be concluded that a thin layer highly doped with cryptophane-A can provide high sensitivity with fast response time. To study this further, measurements of sensitivity and response time with a highly doped cryptophane-A thin layer were done. The measurement data for highly doped cryptophane-A are listed in Table 4.4. The response time can be kept at few seconds with deposition of a thin layer of highly doped SAN. We found that the sensitivity with 33% cryptophane-A and 60 nm is almost the same as the sensitivity with 11 % cryptophane-A and 260 nm thick, while the response time was found to be four times shorter as shown in Table 4.5.

Table 4.4 Measurement data for thin layer of SAN highly doped cryptophane-A

Concentration of cryptophane-A (%)	Thickness (nm)	Sensitivity(x10^{-3}) rad/ppm	Response time (s)
33	60	0.2977	3.4
50	95	0.4374	10

50	170	0.8206	44.5

Table. 4.5 Comparison between thick layer of 11 % and thin layer of 33 % cryptophane-A doped SAN

Concentration of cryptophane-A (%)	Thickness (nm)	Sensitivity($x10^{-3}$) rad/ppm	Response time (s)
11	260	0.3446	14
33	60	0.2977	3.4

In order to analyze the sensitivity as a function of cryptophane-A concentration, all experimental data have been fitted by equation 4.6, where the term $\frac{\partial n_{eff1}}{\partial n_1}$ was obtained from Fimmwave simulations (done by Dr. Jana Jágerská) as discussed in Sec. 4.1.2.1, and the unknown term $\frac{\partial n_1}{\partial x}$ was approximated as: $p.\frac{\partial n_{1(SAN)}}{\partial x} \approx p(n_{CH_4} - n_{N_2})$. Here p represents the sensitivity enhancement due to cryptophane (so-called pre-concentration), and it was used as a fitting parameter. The results are shown in Fig. 4.4.

The simulation of the term $\frac{\partial n_{eff1}}{\partial n_1}$ also allows us to normalize the experimentally measured sensitivities presented in Tables 4.1-4.5 to one common thickness of the sensitive layer. This is done by moving along the fitted curves of Fig. 4.4. The sensitivity for a fixed thickness of 300 nm as a function of Cryptophane-A concentration is shown in Fig. 4.5. The value for pure SAN was taken from previously reported results (i.e. 0.015 x 10^{-3} rad/ppm) [24].

The sensitivity shows a linear trend

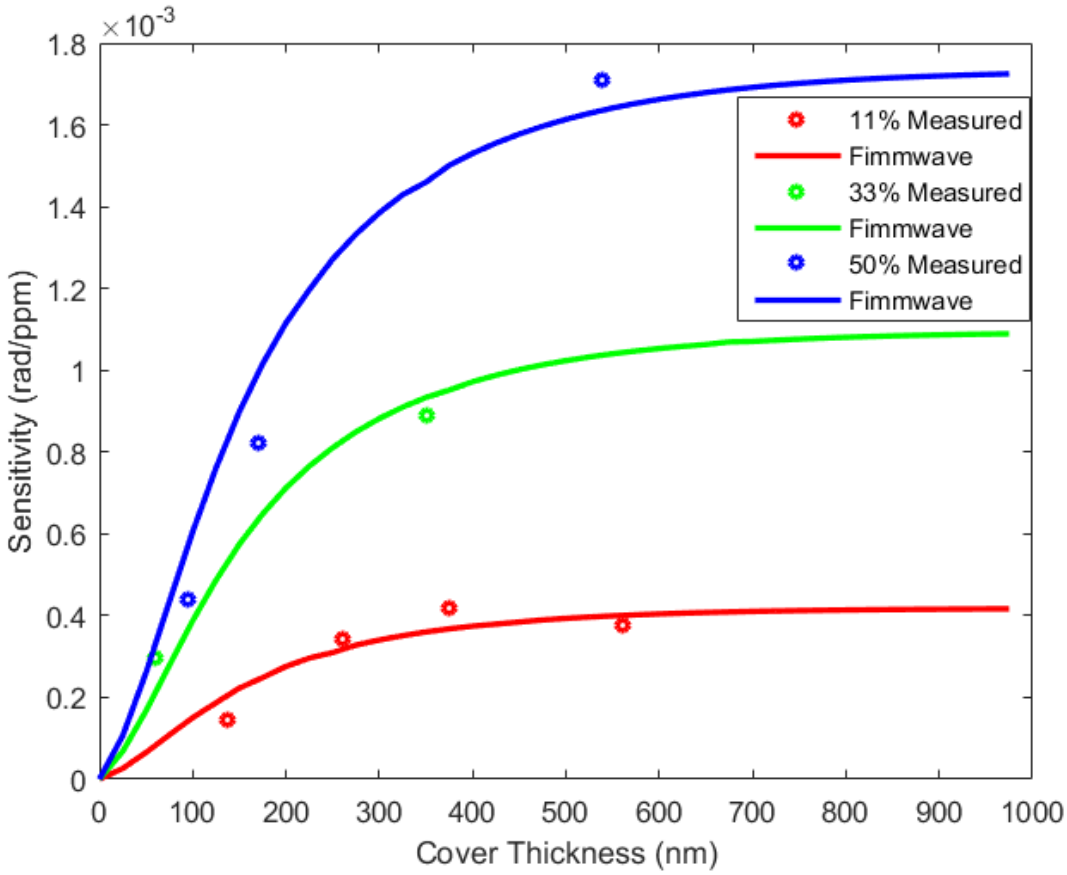

Fig 4.4 Simulated and measured sensitivity (from all tables) vs cover thickness

$$S = a + b.c = 2.2X10^{-5}+2.7X10^{-3}.\text{c} \qquad 4.14$$

Where c is the concentration of cryptophane-A. In the equation 4.14, the first term represents the sensitivity of pure SAN where the concentration of cryptophane-A is equal zero. Note that its value compares well to the theoretical value of $1.7\,X10^{-5}$ found in Section 4.1.2.2.1. However, for cryptophane-A concentrations above 10.5% as discussed in this work, the sensitivity is clearly dominated by the second term related to methane pre-concentration.

.

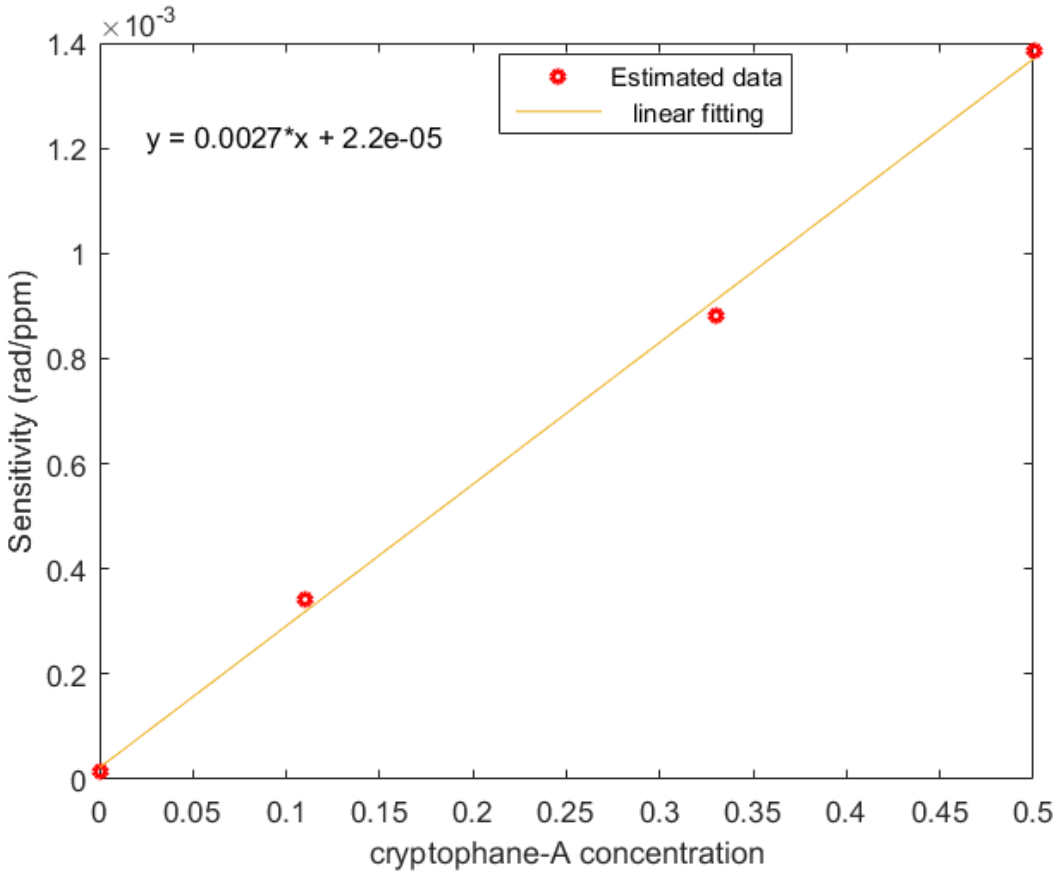

Fig 4.5 Sensitivity vs cryptophane-A concentration

Regarding the response time, a quadratic function from Fick's law gave a good fit for the measurements for 11% cryptophane-A as shown in Fig. 4.3, as well as for other concentrations of cryptophane-A as shown in Fig. 4.6.

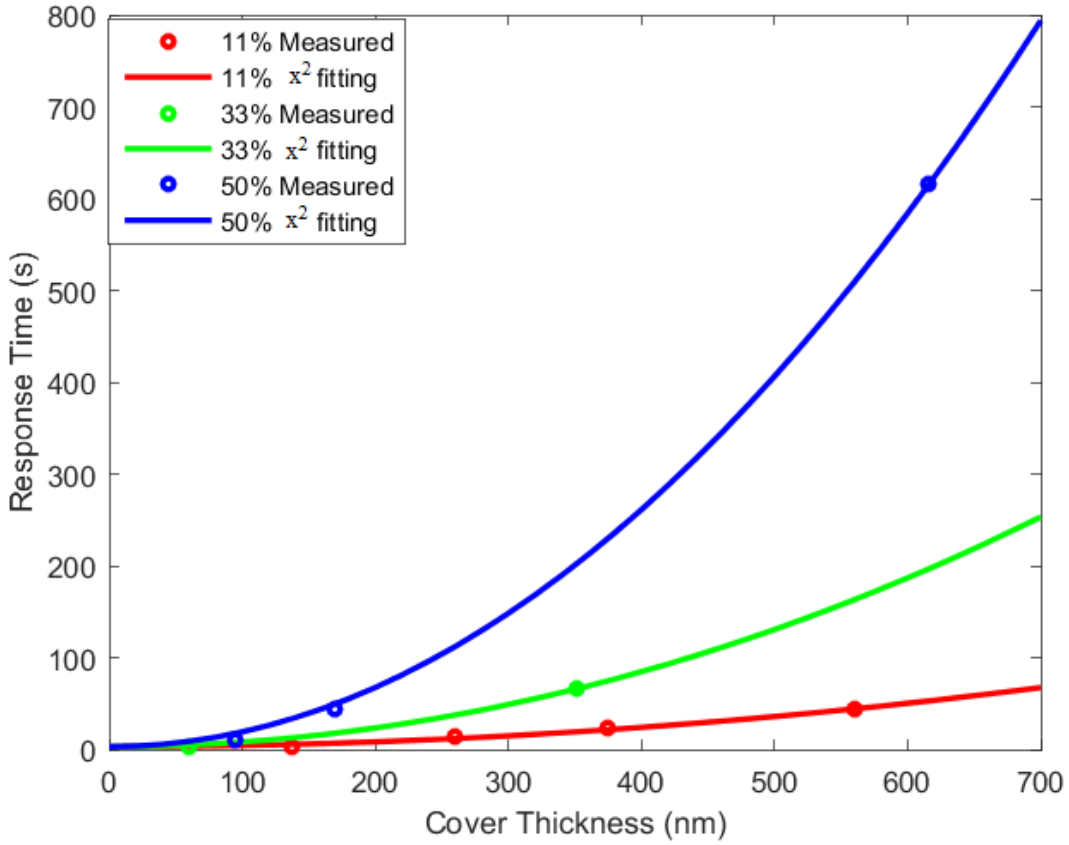

Fig 4.6 Response time vs cover thickness

Based on Fig. 4.4 and 4.6, the thickness and cryptophane-A concentration of the sensitive layer can be selected to best fulfill our requirements of high sensitivity and short response time. An 80 nm thin layer of 50% cryptophane-A doped SAN was chosen as optimal, as it provides good sensitivity and response time of only 3 sec.

The calculation of diffusion coefficient and system response time was also done based on results in Fig 4.6, and the resulting diffusion coefficient for different concentrations of cryptophane-A are listed in Table 4.6.

Table 4.6 Concentration of cryptophane-A vs estimated diffusion coefficient

Cryptophane-A conc. (%)	Diffusion coefficient (nm^2/s)
11	24×10^4
33	6.1×10^4
50	1.9×10^4

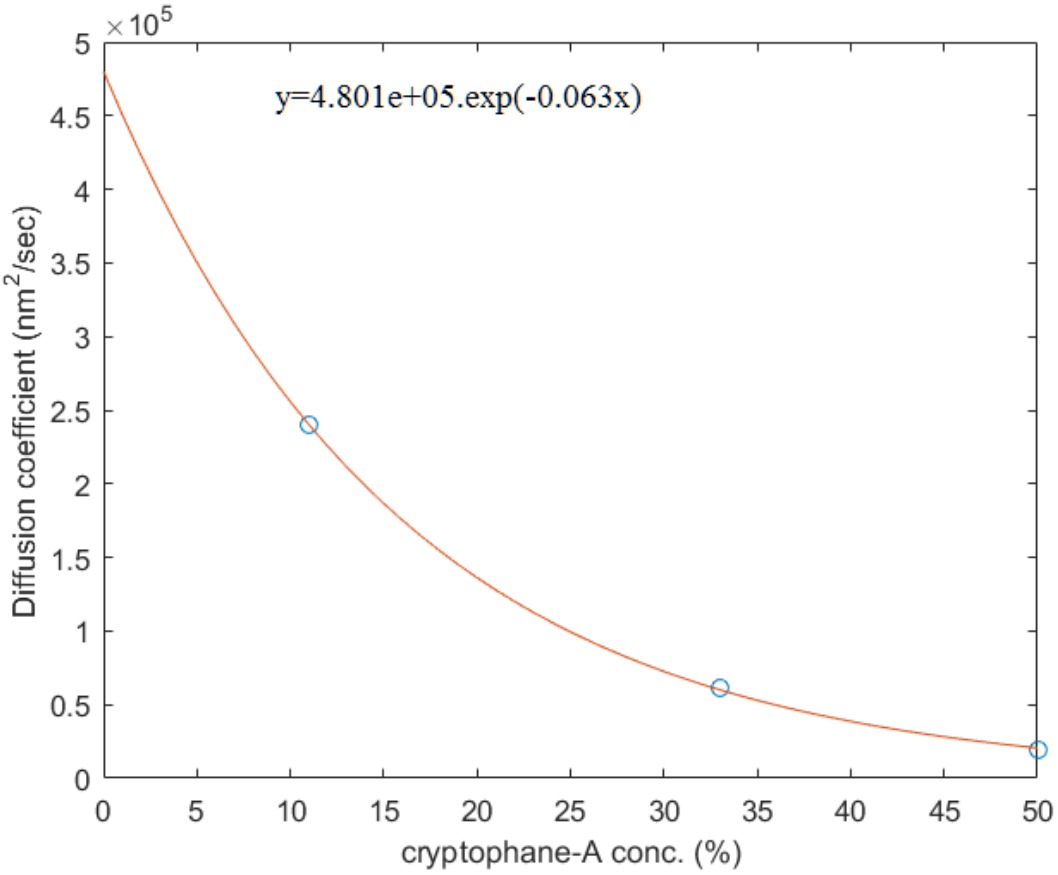

Fig 4.7 Cryptophane-A conc. Vs Diffusion coefficient

The diffusion coefficients for different concentrations of cryptophane-A were plotted versus the concentration of cryptophane-A (Fig. 4.7), in order to study the effect of cryptophane-A on the diffusion of methane. The diffusion coefficients were found to be decreasing very fast (exponentially) with increase in concentration of cryptophane-A, which suggest that the trapping of methane molecules becomes very prominent resulting in slow response time as shown in Fig. 4.6.

Chapter 5

Sensitive layer covered with an insensitive layer

In this chapter, we present the measurement results for increase in sensitivity with deposition of 1µm thick layer of Poly dimethyl siloxane (PDMS) polymer on top of thin sensitive layer (Fig. 5.1). The PDMS layer was deposited on the top because the refractive index of PDMS is higher in comparison to air. So, we expected that the increase in refractive index of top surface might increase the mode overlap in the sensitive layer. And the diffusion coefficient of methane in PDMS is 119 x 10^8 nm^2/s, which is approximately 3 order higher than the measured diffusion coefficient for SAN doped with 11% cryptophane-A ($2.6x10^5 nm^2/sec$). So, it was also expected that the diffusion of methane in PDMS will not slow down the response time of the sensor.

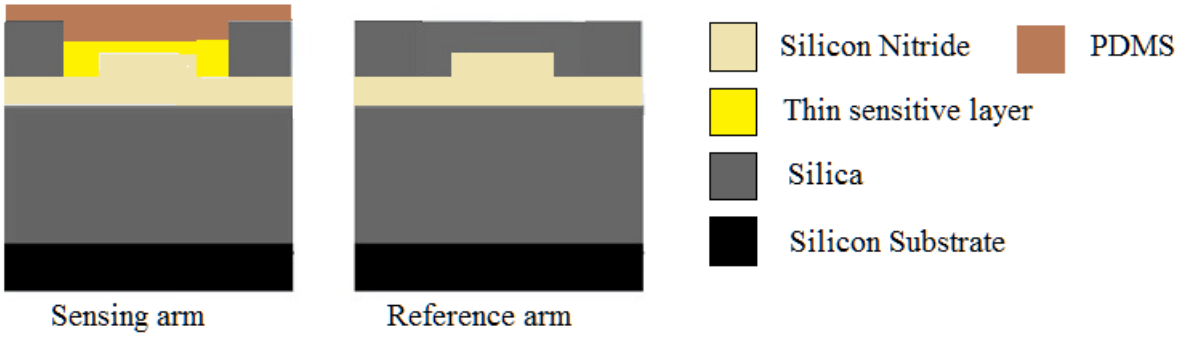

Fig 5.1. Schematic of sensitive layer covered with PDMS layer

The experiment results for response time and sensitivity of thin layer highly doped with cryptophane-A with PDMS on top are presented in Table 5.1.

Table 5.1 Measured values of sensitivity and response time with PDMS and without PDMS

Cryptophane-A conc.	Thickness (nm)	Sensitivity without PDMS (rad/ppm)	Response time without PDMS (s)	Sensitivity with PDMS (rad/ppm)	Response time with PDMS (s)
33%	60	0.29	3.4	0.29	3.4
50%	95	0.437	10	0.645	7.5

From measurement results listed in Table 5.1, we found that the sensitivity was increased with deposition of PDMS on top of thin layer of SAN doped with 50% cryptophane-A, which was expected but for 33%, the sensitivity was not increased, it remained same. We found that the measured signal for 33% without PDMS was very noisy which resulted in uncertainty in exact phase change as shown in Fig. 5.2.

The response time was also decreased with deposition of PDMS on top of thin layer of SAN doped with 50% cryptophane-A, it can also be explained with the reduction in noise level as shown in Fig. 5.2.

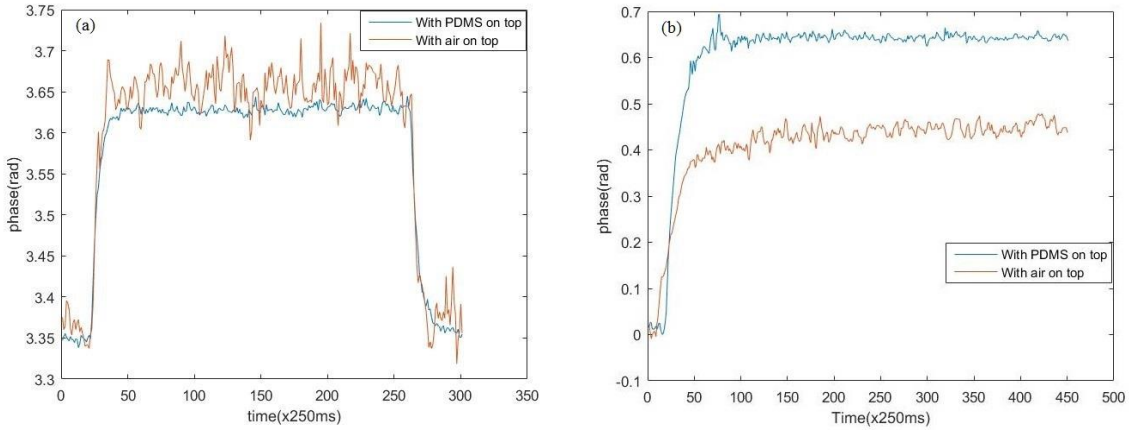

Fig 5.2 (a) Phase change with and without PDMS on the top of 60 nm thin layer with 33% doping. (b) Phase change with and without PDMS on the top of 95 nm thin layer with 50% doping. The phase change measurement was done for 1000 ppm methane.

In order to understand the change in sensitivity with deposition of PDMS layer, the simulation of sensitivity change with cover thickness (33% doped) with PDMS on top and without PDMS was done. The simulations were done by Dr. Jana Jagerska. The simulation results are shown in Fig. 5.2. From simulation results, we found that the sensitivity for thin layer increases with PDMS. The simulation results also show that the sensitivity increase for cover thickness close to 50 nm, is low in comparison to 100 nm. Which justifies measured sensitivity for 33% cryptophane-A.

From these measurement results we found that deposition of PDMS, increases the sensitivity without affecting the response time. In addition, the PDMS layer reduces the noise level present in the thin layer measurement and make the sensor much more stable.

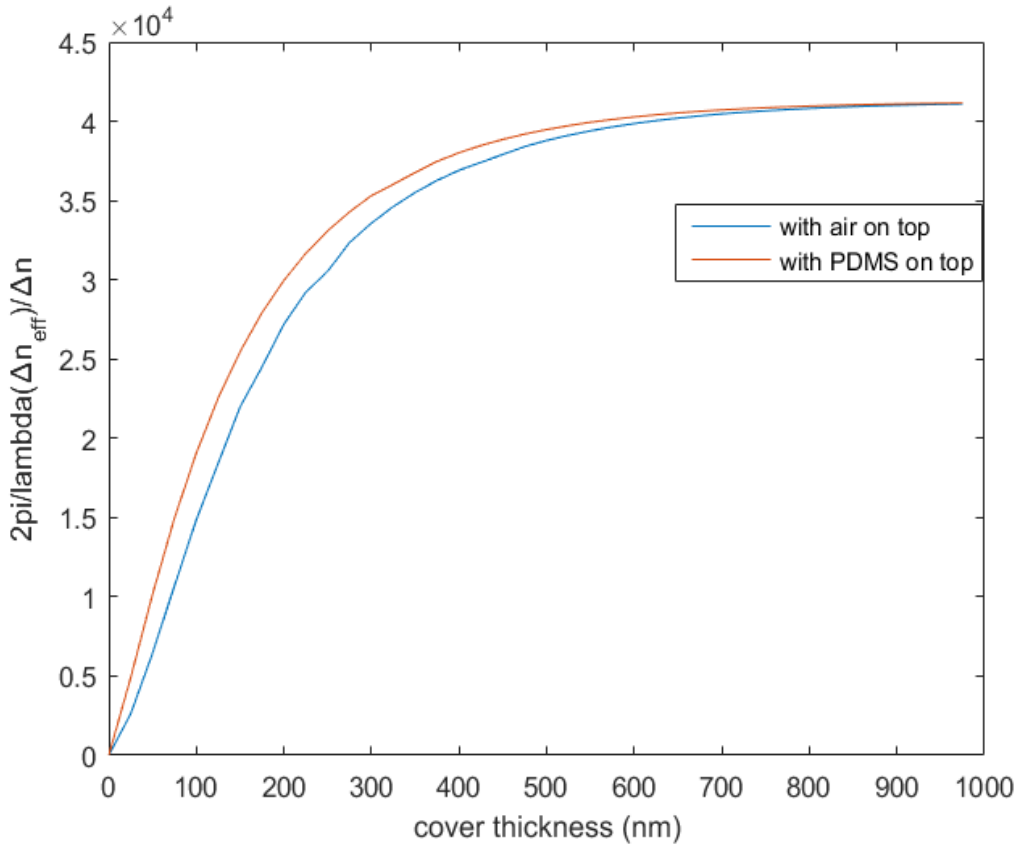

Fig 5.2 Simulation of sensitivity change with cover thickness for 1µm thick PDMS on top and without

Chapter 6

Balanced interferometer with doped and undoped layers on the waveguide arms

In previous chapter, we presented the increase in the sensitivity of the optimum thickness of sensitive layer without effecting the response time. Which makes the highly sensitive with fast response time. This chapter presents the enhancement in stability and the selectivity to methane sensor.

The existing sensor suffers from long-term drift which affects the repeatability of the sensor during long measurements. The long-term drift in existing sensor comes from the temperature sensitivity of the sensor as the sensor has silica in reference arm, which is methane impermeable but it has very low thermo-optical coefficient ($12.9 \times 10^{-6}K^{-1}$). On the other hand, sensing arm is cladded with polymer which has very high thermo-optical coefficient ($-110 \times 10^{-6}K^{-1}$) [23]. So, difference in thermo-optical coefficient of both arms makes the sensor sensitive to temperature. To reduce the temperature sensitivity of the chip, the peltier element is placed below the chip, which regulates the temperature of the chip from below. But the polymer layer with very high thermo-optical coefficient is deposited on the top, so the small variation in the temperature of the gas flowing above the chip results in phase change. In the lab, temperature change is very slow, so during the measurement the sensitivity of methane overtakes the sensitivity due to slow change in temperature. But, in long measurements it results into a slow drift. And it was also observed that the measurements which were done in the night, the measurements were without drift. Which also shows that the drift reduces when temperature is stable (night).

In order to reduce the slow temperature drift, we decided to improve the sensor with development of sensor from balanced Mach-Zehnder interferometer. Because in balanced interferometers both arms are covered with the material having similar physical and optical properties, so that the undesired sensitivity get cancel out at the output. To make balanced Mach-Zehnder interferometer, we decided to deposit the SAN layer on one arm of the interferometer and SAN doped with cryptophane-A doped on the other. For that we assumed that the thermo-optical properties of the both arms are same. In addition, with the deposition of SAN in one arm and SAN doped with cryptophane in another arm, it was expected that the

selectivity of the sensor will increase. Because with deposition of SAN in reference arm the sensitivity of SAN for different gases cancels out from both arms which makes the sensor highly sensitive to methane.

The measurement results for methane sensitivity and stability are described in next section.

6.1 Methane sensitivity

For methane sensitivity measurement, first the 80 nm thin layer of SAN was deposited on the whole chip as there was problem in directly plotting the polymer layer in sensing windows of interferometer (discussed in chapter 3). Then, on the top of the thin layer of SAN, 400 nm thick layer of 25% cryptophane-A doped SAN was deposited (plotted) on sensing arm and pure SAN of 400 nm thickness was deposited on reference arm. The deposition of SAN and SAN doped cryptophane-A was done on 0.5 long open window in both arms. The measurement results for 1000 ppm and 40000 ppm methane are shown below in Fig. 6.1.

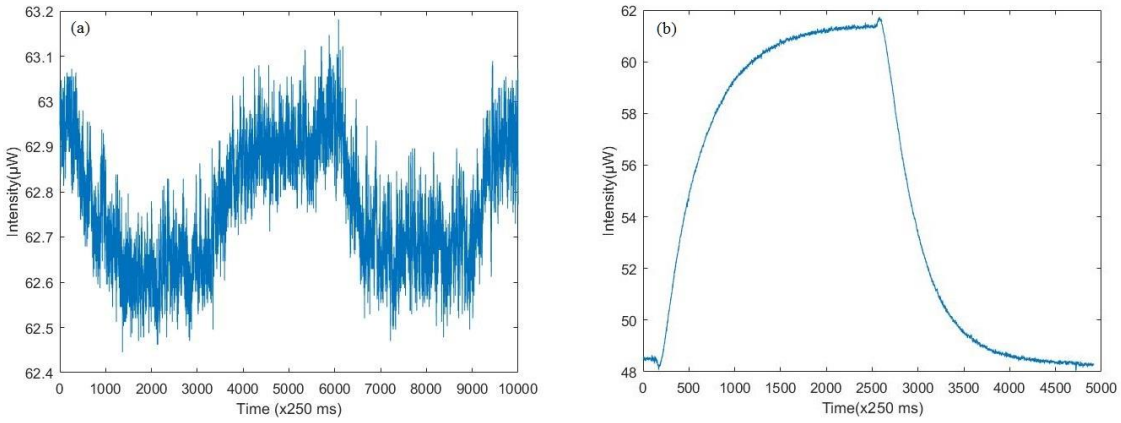

Fig 6.1 (a) Measured output intensity for alternate switching of 0 to 1000 ppm methane (b) Measured output intensity for alternate switching of 0 to 40000 ppm methane.

From measurement results, we found that the sensor with balanced Mach-Zehnder interferometer was sensitive to methane. The sensitivity was found to be very low because the interaction length for the sensor was only 0.5 cm.

As shown in Fig. 6.1 (b), we measured an unexpected dip in intensity when gas was switched from nitrogen to methane (40000). The measured dip in the intensity was not very fast, so it suggests that it was not happening because of pressure change.

Theoretically, we explained this dip with difference in diffusion rate of methane in pure SAN and doped SAN. It was already shown in previous chapters that the response time for diffusion

of methane in SAN doped with cryptophane-A is very slow. While diffusion of methane in pure SAN polymer is very fast [24]. So, when methane gas is introduced in the system, intensity changes due to sensitivity of SAN to methane and after few seconds the sensitivity of doped SAN overtakes the sensitivity of pure SAN. Which results in the dip shown in Fig. 6.1(b). The dip corresponds to the sensitivity of pure SAN.

And in order to mathematically support this argument, the ratio of intensity change due to dip and methane was calculated.

$$\text{Ratio}=\frac{(\,intensity\ change\ due\ to\ methane)}{intensity\ change\ in\ kink}=\frac{61.52-48.54}{48.42-48.09}=39.3$$

The ratio should corresponds to the pre-concentration factor for 25% cryptophane-A (Fig.4.5), because if the dip corresponds to the sensitivity of SAN. The calculated value was found to be low in comparison to estimated value from chapter 4, which is approximately 50. But in starting, we mentioned that the thin layer (80 nm) of pure SAN was deposited below the sensitive layer, by considering that the most part of evanescent field was confined in thin layer of SAN. The lower value of pre-concentration can be justified.

From, this measurement we found that the sensor is highly selective to methane, the dip suggests that the sensitivity of pure SAN was cancelling out from both arms with delay.

During these measurements, the phase sensitivity was not calculated because for phase sensitivity calculation, values of maximum and minimum intensity are required. And with 1000 ppm and 40000 ppm we were not able to reach the maxima. The temperature scan was also done to attain the maxima or minima of the intensity. But temperature change was giving very small intensity change in comparison to methane. Which shows that the sensor is very less sensitive to temperature that is required in reducing the long-term drift from the existing sensor. To estimate the long-term drift and stability of the developed sensor is described in next section.

6.2 Stability

To investigate the stability improvement from the existing senor, the 40 min long intensity measurement for balanced and unbalanced interferometer was compared as shown in Fig.6.2.

The measurement data of unbalanced Mach-Zehnder interferometer with 351 nm thick layer of 33% cryptophane-A doped SAN and balanced Mach-Zehnder interferometer with 400 nm thick layer of SAN on one arm and SAN doped with 25% cryptophane-A in other arm were compared to estimate the stability improvement. The sensing window in balanced Mach-Zehnder was 0.5 cm long and in unbalanced interferometer it was 3 cm long. For comparison, the slopes for both measurement data were scaled to same sensing window length (i.e. 0.5 cm).

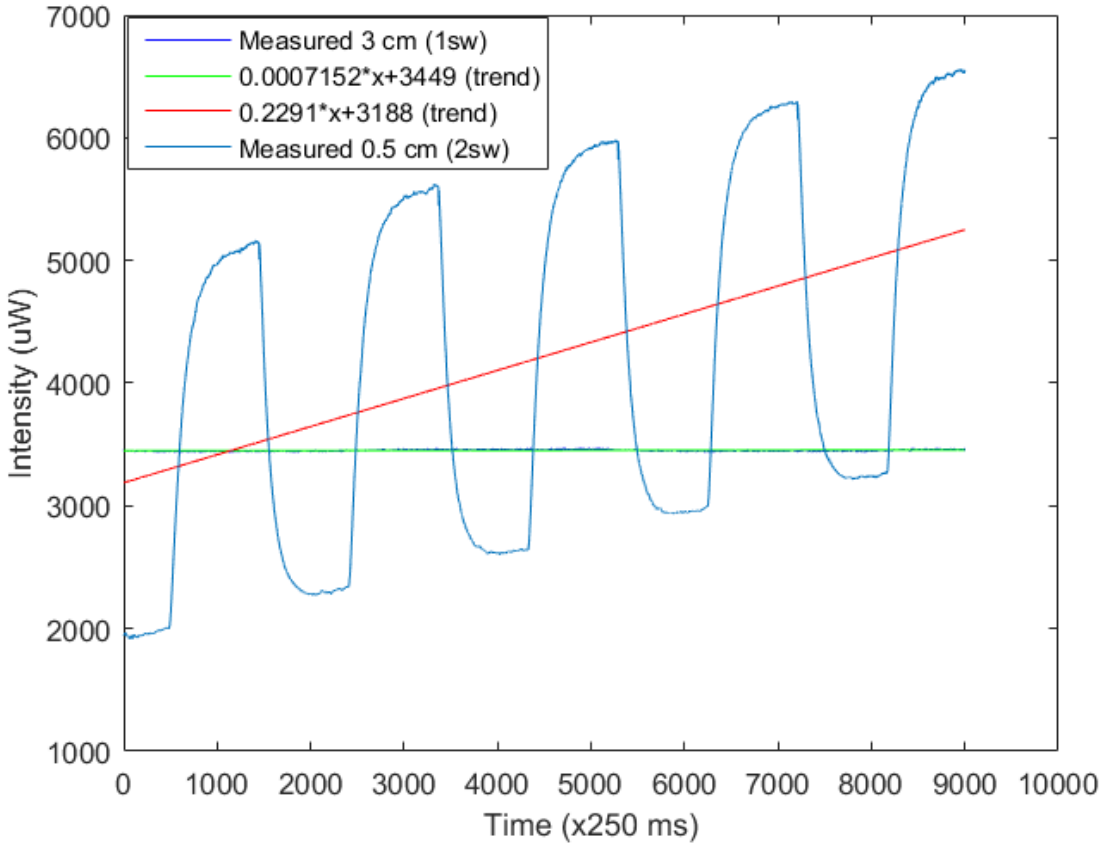

Fig. 6.2 The stability comparison between sensing with balanced and unbalanced Mach-Zehnder interferometer.

The slope of drift in unbalanced Mach-Zehnder interferometer, when scaled to 0.5 cm interaction length was found to be 9.16 microwatt/min.

Similarly, the slope of drift for balanced Mach-Zehnder interferometer was calculated as 0.17 microwatt/min.

From calculated slope (per minute), the drift in unbalanced Mach-Zehnder interferometer was found to be 50 times more than the balanced Mach-Zehnder interferometer. Which shows that the balanced Mach-Zehnder interferometer provides much better stability to the sensor.

From measurement results, we found that the sensor with balanced Mach-Zehnder interferometer provides high stability and selectivity to methane. And with combination of results from this chapter and last chapter, a sensor can be developed with high sensitivity, fast response time and high stability.

Chapter 7

Conclusion and future work

7.1 Conclusion

This thesis describes the optimum thickness of SAN polymer highly doped with cryptophane-A for sensing of methane, which provides high sensitivity and fast response time. The stability and selectivity of the sensor is also described.

First, the highest sensitivity of the developed methane sensor was investigated. The results showed that the 2-fold sensitivity enhancement than the previously reported sensitivity. But this increase in sensitivity comes in the expense of slow response time.

Second, the change in response time and sensitivity with cover thickness was investigated. The results showed that the response time and sensitivity both were increasing with increase in cover thickness. Then, measurement results with thin layer of highly doped cryptophane-A showed that the thin layer of highly doped cryptophane-A can be considered as optimum thickness as it fulfills our requirement of highly sensitive and fast sensor. The 80 nm thin layer of cryptophane-A doped SAN was chosen as optimum thickness for developed sensor.

Third, the sensitivity and noise associated with thin layer of SAN highly doped with cryptophane-A was investigated by deposition of PDMS layer on the top of the thin layer. The results showed that the sensitivity and noise level was improved, which was further supported by simulation results.

After optimization of thickness of sensitive layer, the long term stability of the sensor was investigated by implementation of balanced Mach-Zehnder in place of unbalanced Mach-Zehnder. For fabrication of balanced Mach-Zehnder interferometer, photolithography process was used to deposit Ag in one arm of the balanced interferometer to deactivate one arm for methane. But we found that the available solvents and photoresist are not compatible with polymer. Then, Microplotter II was used for deposition of SAN in one arm and doped SAN in other arm. The measurement results with balanced Mach-Zehnder interferometer plotted with Microplotter II showed that the stability is much better than the unbalanced one. And in addition, it can increase the selectivity towards as sensitivity of SAN for other gases will cancel out from both branches.

Based on the measured, the suggested sensor can be developed with the deposition of 20 nm thin layer of SAN on the chip, followed by plotting of doped and undoped SAN on both arms and covered with 1μm thick layer of PDMS.

7.2 Future work

To further improve the sensor, measurements with thin layer of doped and undoped SAN on balanced Mach-Zehnder interferometer with large sensing window can be done. Then, the selectivity of the balanced Mach-Zehnder interferometer can be verified by introducing the sensor with mixture of gases. Finally, the sensor can be mounted on the drone for testing after inclusion of fiber-pigtailing at input/output of the chip and packaged electronics.

Appendix 1

Accepted abstract for CLEO Europe-2017

Sensitivity and Response time of an On-Chip Methane Sensor

Mukesh Yadav[1], Jana Jágerská[1], Jørn H. Hansen[2] and Olav Gaute Hellesø[1]

1. *Dept. of Physics and Technology, UiT The Arctic University of Norway, 9037 Tromsø, Norway*
2. *Dept. of Chemistry, UiT The Arctic University of Norway, 9037 Tromsø, Norway*

In recent years, methane detection has become a hot topic due to the strong impact of methane on the global warming and the climate change. There has also been rising interest in the development of new methane sensors that can tackle the task of sensitive atmospheric methane detection, but are smaller, lighter, and cheaper than the state of the art. Our approach to this challenge is the development an on-chip waveguide sensor, which compensates for the rather short path lengths possible on a chip with pre-concentration of methane in a thin, specially designed waveguide cladding layer.

Our detection technique is based on evanescent refractive index sensing with a Silicon Nitride shallow rib-waveguide Mach-Zehnder interferometer, see Figure 1a). The waveguide was fabricated with dimensions supporting single TE and TM modes at the wavelength of 785 nm. The reference arm is cladded with SiO_2 that is impermeable to methane, and the sensing arm is cladded with Styrene Acrylonitrile (SAN) polymer doped with Cryptophane-A. Cryptophane-A is a molecular compound, which has a high affinity towards methane, i.e., it acts as a host cavity encapsulating methane and binding it within with weak dispersion forces. We have previously reported that the presence of cryptophane increases the methane concentration in the SAN layer by a factor of 50 for the crytophane:SAN mixing ratio of 1:3. With this concentration we achieved a limit of detection of 6 ppm [1], which is 1-2 orders of magnitude better than what is typical with other methane sensors in a similar size and price range.

However, in order to bring the methane sensor to the field, not only sensitivity but also specificity to methane and the sensor response time need to be quantified. The latter is directly related to the diffusion mechanism of methane in cryptophane-doped polymers, which has up to date never been closely investigated or reported. In this paper we provide the first experimental study of methane diffusion in strongly doped cryptophane layers. Our data represent an important step towards understanding and optimization of the response time of cryptophane-doped on-chip sensors, which is crucial for their future deployment in practical applications

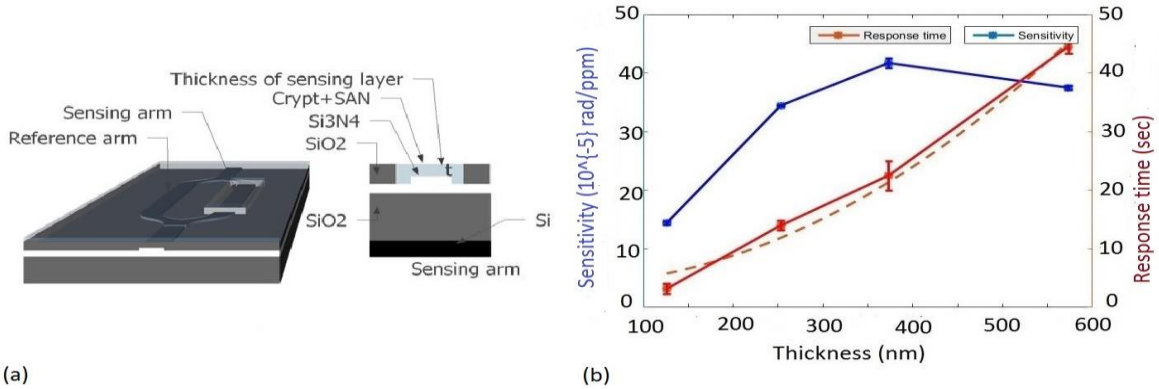

Fig. 1. a) Schematic of the waveguide chip. b) Sensitivity and response time versus the sensing layer thickness.

Figure 1b) shows the first experimental data, where the sensitivity and the response time were measured for four different thicknesses of the sensing layer with cryptophane:SAN concentration of 8.5. Although both sensitivity and response time increase with thickness, it is evident that the sensitivity gets saturated for a thickness of about 300 nm, while the response time continues to increase. From the measured response times, the diffusion coefficient was estimated to 2.6 x 10^{-9} cm^2/sec. This estimate shows that the diffusion in the sensing layer is considerably slower, by 3 orders of magnitude, than in pure polymers (SAN, PDMS, PPMS, etc.) [3]. Optimization of the sensor performance will be discussed, including approaches for making a fast and sensitive sensor for atmospheric methane. Development of a prototype will be outlined.

References

[1] J. Jágerská, F. T. Dullo, M. Ingvaldsen, S. Lindecrantz, M. Engqvist, J. Hansen, and O. G. Hellesø, "On-Chip Methane Sensing with Cryptophane-A Cladded Waveguide Interferometers," in *Conference on Lasers and Electro-Optics*, OSA Technical Digest (2016) (Optical Society of America, 2016), paper SF2H.3.

[2] F. T. Dullo, S. Lindecrantz, J Jágerská, J. H. Hansen, M. Engqvist, S. A. Solbø, and O. G. Hellesø, "Sensitive on-chip methane detection with a cryptophane-A cladded Mach-Zehnder interferometer," Opt. Express **23**, 245563 (2015).

[3] S.G. Charati and S. A. Stern, "Diffusion of Gases in Silicone Polymers: Molecular Dynamics Simulations," Macromolecules **31(16),** 5529-5535 (1998)

Appendix 2

List of parts

Item	Manufacturer	ID
Optical table	Standa	1VIS95W
Laser	Crystalaser	DL785-120-S0
Half-wave plate	Thorlabs	
Beam expander lens 1	Thorlabs	AC254-030-B-ML
Beam expander lens 2	Thorlabs	LA1986-A
Polarizer	Thorlabs	LPVIS100-MP
Objective lens input	Leitz Wetzlar	569244
Objective lens output	Thorlabs	UIS 2 PLN10X
Photodetector	Thorlabs	SM1PD1A
Camera	Allied Vision	GC2450
Piezo translation stage	Thorlabs	MAX302/M
Piezo controller	Thorlabs	MDT 693A
Modular Rack Chasis	Thorlabs	PRO8000
Photocurrent measurement card	Thorlabs	PDA8000-2
Peltier	Laird Technologies	430139-513
Temperature controller	Thorlabs	TED8080
MFC 100 ml/min x2	Bronkhost	F-201-CV-100-AAD-11-V

Vaccum pump	VWR	PM20405
Gas	AGA	Nitrogen
Gas	AGA	1000 ppm in nitrogen

Bibliography

1. https://www.epa.gov/ghgemissions/overview-greenhouse-gases
2. https://www.esrl.noaa.gov/gmd/aggi/aggi.html
3. Kirschke, Stefanie, et al. "Three decades of global methane sources and sinks." *Nature Geoscience* 6.10 (2013): 813-823.
4. Liu, Xiao, et al. "A survey on gas sensing technology." *Sensors* 12.7 (2012): 9635-9665.
5. Sohler, W. "Integrated optics in LiNbO 3." *Thin Solid Films* 175 (1989): 191-200.
6. Bogue, Robert. "Fibre optic sensors: a review of today's applications." *Sensor Review* 31.4 (2011): 304-309.
7. Mukundan, Harshini, et al. "Waveguide-based biosensors for pathogen detection." *Sensors* 9.7 (2009): 5783-5809.
8. Heideman, R. G., and P. V. Lambeck. "Remote opto-chemical sensing with extreme sensitivity: design, fabrication and performance of a pigtailed integrated optical phase-modulated Mach–Zehnder interferometer system." *Sensors and Actuators B: Chemical* 61.1 (1999): 100-127.
9. Kozma, Peter, et al. "Integrated planar optical waveguide interferometer biosensors: A comparative review." *Biosensors and Bioelectronics* 58 (2014): 287-307.
10. Dullo, Firehun Tsige, et al. "Sensitive on-chip methane detection with a cryptophane-A cladded Mach-Zehnder interferometer." *Optics express* 23.24 (2015): 31564-31573.
11. Dullo, Firehun Tsige, et al. "Single-Mode Limit and Bending Losses for Shallow Rib Si_3N_4 Waveguides." IEEE Photonics Journal 7.1 (2015): 1-11.
12. Lafleur, Josiane P., et al. "Recent advances in lab-on-a-chip for biosensing applications." Biosensors and Bioelectronics 76 (2016): 213-233.
13. Zinoviev, Kirill E., et al. "Integrated bimodal waveguide interferometric biosensor for label-free analysis." Journal of Lightwave Technology 29.13 (2011): 1926-1930.
14. Bogue, Robert. "Fibre optic sensors: a review of today's applications." Sensor Review 31.4 (2011): 304-309.
15. Hill, Ryan T. "Plasmonic biosensors." Wiley Interdisciplinary Reviews: Nanomedicine and Nanobiotechnology 7.2 (2015): 152-168.
16. Hunsperger, Robert G., and Jurgen R. Meyer-Arendt. "Integrated optics: theory

and technology." *Applied Optics* 31 (1992): 298.
17. Ikkink, Teunis Jan. *Interferometric interrogation concepts for integrated electro-optical sensor systems*. Universiteit Twente, 1998.
18. Prieto, Francisco, et al. "An integrated optical interferometric nanodevice based on silicon technology for biosensor applications." *Nanotechnology* 14.8 (2003): 907.
19. Dante, Stefania, et al. "All-optical phase modulation for integrated interferometric biosensors." *Optics express* 20.7 (2012): 7195-7205.
20. Ymeti, Aurel, et al. "Integration of microfluidics with a four-channel integrated optical Young interferometer immunosensor." *Biosensors and Bioelectronics* 20.7 (2005): 1417-1421.
21. Ymeti, Aurel, et al. "Fast, ultrasensitive virus detection using a Young interferometer sensor." *Nano letters* 7.2 (2007): 394-397.
22. Jágerská, Jana, et al. "On-chip methane sensing with cryptophane-A cladded waveguide interferometers." CLEO: Science and Innovations. Optical Society of America, 2016.
23. Dullo, Firehun Tsige, et al. "Temperature Sensitivity of a Waveguide Young Interferometer." IEEE Photonics Technology Letters 28.11 (2016): 1205-1208.
24. Ingvaldsen, Martin. *Sensitivity to pressure and methane of a cryptophane-A doped polymer*. MS thesis. UiT Norges arktiske universitet, 2015.
25. Charati, S. G., and S. A. Stern. "Diffusion of gases in silicone polymers: molecular dynamics simulations." *Macromolecules* 31.16 (1998): 5529-5535.
26. https://en.wikipedia.org/wiki/Fick%27s_laws_of_diffusion
27. Souteyrand, E., et al. "Behaviour of cryptophane molecules in gas media." *Sensors and Actuators B: Chemical* 33.1-3 (1996): 182-187.
28. https://en.wikipedia.org/wiki/Henry%27s_law